

~~193~~
65-RF/AK80

DEPARTMENTS OF
ATMOSPHERIC SCIENCES AND OCEANOGRAPHY
UNIVERSITY OF WASHINGTON

SCIENTIFIC REPORT NO, 18
OFFICE OF NAVAL RESEARCH
CONTRACT **N00014-76-C-0234**
NR 307-252

AND

BLM/NOAA
CONTRACT NO, 03-5-022-67, RU 87"

A FIELD STUDY OF THE PHYSICAL PROPERTIES,
RESPONSE TO SWELL, AND SUBSEQUENT FRACTURE OF A
SINGLE ICE FLOE IN THE WINTER BERING SEA

BY

VERNON A, SQUIRE

AND

SEELYE MARTIN

JULY 1980

A FIELD STUDY OF THE PHYSICAL PROPERTIES,
RESPONSE TO SWELL, AND SUBSEQUENT FRACTURE OF A
SINGLE ICE FLOE IN THE WINTER BERING SEA

BY

VERNON A, SQUIRE
SCOTT POLAR RESEARCH INSTITUTE
LENSFIELD ROAD, CAMBRIDGE
CB2 1ER ENGLAND

AND

SEELYE MARTIN
DEPARTMENT OF OCEANOGRAPHY
UNIVERSITY OF WASHINGTON
SEATTLE, WASHINGTON 98195

REPRODUCTION IN WHOLE OR IN PART
IS PERMITTED FOR ANY PURPOSE OF THE
UNITED STATES GOVERNMENT

ABSTRACT

Surface strain and vertical heave response experiments were conducted for a single floe within the marginal ice zone of the winter Bering Sea. The strain was measured using an array of three strainmeters placed in a 120° rosette configuration, and the heave was computed from simultaneous records of vertical acceleration on the floe and in the water around the floe. Physical properties studies and underwater traverses by divers were also carried out for the floe. The data are presented and interpreted in the light of the subsequent floe fracture; the mean fracture strain amplitude ϵ is found to lie between 44 and 85 μ strain. A discussion of the directionality of the wave energy during the experiment is also given.

TABLE OF CONTENTS

	Page
LIST OF FIGURES	iii
INTRODUCTION	1
INSTRUMENTS	11
Strainmeters	11
Accelerometers	11
DATA ANALYSIS	13
THE BERING SEA DATA AND THEIR INTERPRETATION	17
Seastate	17
Heave Response	24
The Strain Data	30
DISCUSSION	43
CONCLUSIONS	46
ACKNOWLEDGEMENTS	47
REFERENCES	48
DISTRIBUTION LIST	51
REPORT DOCUMENTATION PAGE	55

LIST OF FIGURES

Figure	Page
1a,b. Aerial photographs of the floe: (a) The floe and its surroundings, (b) a close-up view.	4
2. A map of the floe. F1 and F2 mark the core hole positions; dashed lines BEA , DEC show approximate positions of underwater surveys.	5
3a,b. Surface photographs: (a) Looking down the ridge; (b) the strain rosette.	6
4a,b. Salinity (o), temperature (o), and crystal structure of the ice cores versus depth: (a) F1 , (b) F2 .	8
5. The core photographs: F1 , F2 ; core top is at page top.	9
6a,b. The underwater traverses: (a) Line CED , (b) line BEA .	10
7a,b. Time series and power spectra for two 20 minute Waverider buoy records. Records begin at 10.30 and 10.50 respectively.	19
7c,d. Time series and power spectra for two 20 minute Waverider buoy records. Records begin at 11.12 and 11.32 respectively.	20
7e,f. SEASPRI time series and power spectra for two 30 minute records beginning at 10.38 and 11.08 respectively.	21
7g,h. SEASPRI time series and power spectra for two 30 minute records beginning at 11.56 and 12.26 respectively.	22
8a,b. Time series and power spectra for two 30 minute floe accelerometer records. The records are synchronized with Figure 7e,f.	25
8c,d. Time series and power spectra for two 30 minute floe accelerometer records. The records are synchronized with Figure 7g,h.	26
9a,b. Frequency response functions and coherence functions for floe-mounted accelerometer with reference to SEASPRI buoy.	28
9c,d. Frequency response functions and coherence functions for floe-mounted accelerometer with reference to SEASPRI buoy.	29

Figure		Page
10.	Comparison of experimental and theoretical curves for wavelength versus wave frequency.	31
11a,b.	Strain spectra and time series for strainmeter 2. The time series are synchronized with Figure 7e,f.	33
12a,b,c.	Gain factors for strainmeters 1, 2, and 3 with respect to SEASPRI buoy.	35
13a,b.	Amplitude spectra for principal strains and principal strain direction. Experiments began at a) 10.38 and b) 11.08.	38
13c,d.	Amplitude spectra for principal strains and principal strain direction. Experiments began at c) 11.56 and d) 12.26.	39
14.	Wave steepness necessary to produce strains of 44 and 85 μ strain at surface of the floe as a function of wave period.	44

INTRODUCTION

This report describes a field study of the response to ocean swell and subsequent fracture of an ice floe near the ice edge in the winter Bering Sea. In the Bering Sea the ice edge forms in the following way: First, **McNutt** (1980) shows that the sea ice forms in the northern coastal **polynyas**, from where it is advected southwest as large, km-sized floes by the prevailing northeast winds. As these floes approach the ice edge, the data of Squire and Moore (1980), and **Bauer** and Martin (1980) shows that the ocean swell propagation into the pack fractures the large floes into small floes with horizontal scales of 20-40 m. The combination of wind and swell then acts to raft and ridge these floes, yielding ridges as high as 1 m and keels as deep as 5 m. Because of the combination of increased aerodynamic drag of the ridges and the small floe size, the floes near the edge are blown southwest away from the pack as groups in the form of ice bands measuring about 10 km long by 1 km wide. As they move into warmer water, after one or two days the bands melt. To summarize, the propagation of ocean swell into the pack fractures the large floes and increases their aerodynamic drag, thus leading to their eventual melting. **Wadhams** (1980, page 56) describes a similar process at the Norwegian Sea ice edge, and refers to the edge as an ice "**scrapyard**". Because of these effects, any future numerical model of the ice edge may require in addition to wind, current, and temperature data, information on both ocean swell and floe fracture properties.

To investigate these processes, we carried out a study of the **flexural** properties of a single floe from the NOAA ship **SURVEYOR** during our March 1979 ice edge cruise. We did the experiment on 6 March 1979 at **58°34'N, 167°53'W**, with the ship just within the ice edge. The weather on this day

was good with negligible winds and an air temperature of -7°C at 1000 h local. The study proceeded as follows: In the morning one of us (S.M.) reconnoitered with a small boat the ice floes within a distance of about one nautical mile of the ship. We chose a floe typical of its surroundings with the restrictions that the floe be large enough to support the personnel and, to simplify later comparison with theory, have a minimum of surface relief.

We then landed a party of five on the floe and carried out the following procedures: First, we took two ice cores through the floe and determined the floe thickness to be about 0.3 m. Also, we made a map of the floe surface. Then we deployed three strainmeters in a 120" rosette, a **floe-mounted** accelerometer, and an accelerometer **freely** floating in the water alongside the floe. The data recorded simultaneously from these instruments was used **to** compute the response of the floe to the incident wave energy. The waves force the floe into three bodily motions: heave, surge and sway; three angular oscillations: yaw, pitch and roll; and a flexural mode due to the pressure variation of the propagating wave beneath the floe. The **strainmeter** data give the **flexural** response while the accelerometer data give the heave. The accelerometer in the water and a Waverider buoy deployed from the ship measured the ocean wave spectrum. After these **measurements** were completed, we returned to the ship about 1300 h. Next, in the afternoon during a related ice properties survey, we overflew and photographed the floe. Then one of us (V.S.) returned to the floe with divers from the ship, who surveyed the underside of the floe finding keels of order 4 m in depth. **We** also found that in our absence the ice floe had fractured, so that during the morning experiment the stress must have been very close to the critical fracture value.

To describe our observations in detail, Figures 1a and 1b show two aerial views of the floe, taken from an altitude of about 60 m. The first photograph shows the floe and its surroundings. The second photograph is a closer view, where on the floe surface footprints are clearly visible. We called the dark area toward the camera the "beat"; shortly after this photograph was taken, this end of the floe broke off. Figure 2 shows a map of the floe made from surface measurements. The map shows the location of the beach, and the position of a small crack and a small ridge which ran the length of the floe. The map also shows the location of the **triaxial** strain rosette, the location of the two core holes marked **F1** and **F2**, and the positions where the vertical accelerometers were deployed. Finally, the lines **AEB** and **CED** show the location of the underwater traverses, and the dotted line shows the approximate position of the floe fracture line. Next, Figure 3a shows a surface photograph looking down the small ridge toward the beach, where the flag marks the ridge, and the strain array is to the right. Figure 3b shows a photograph of the strain rosette, and also shows that the floe surface was covered with about 5-10 mm of snow.

To describe the ice properties of the **floe**, we cored the floe in two **places** with a **SIPRE** corer and measured the ice temperature, salinity, and crystal structure. To determine the temperature, we placed the ice core in an insulated box cut to fit snugly around a **SIPRE** core, drilled into the side of the core through preset holes, and measured its temperature profile with a thermistor. We then cut the core vertically in half. One half was cut into 50 mm vertical sections which we separated and placed into plastic bags for later salinity analysis on board the ship. The other **half** was both photographed and used to determine the distribution of **frazil** and columnar ice with depth.

1. The first part of the document discusses the importance of maintaining accurate records of all transactions and activities. It emphasizes the need for transparency and accountability in financial reporting.

2. The second part of the document outlines the various methods and techniques used to collect and analyze data. It includes a detailed description of the experimental procedures and the statistical analysis performed.

3. The third part of the document presents the results of the study, including a comparison of the different methods and techniques used. It also discusses the implications of the findings and the potential applications of the research.

4. The fourth part of the document provides a conclusion and a summary of the key findings. It also includes a list of references and a list of figures and tables.

1. The first part of the document discusses the importance of maintaining accurate records of all transactions and activities. It emphasizes the need for transparency and accountability in financial reporting.

2. The second part of the document outlines the various methods and techniques used to collect and analyze data. It includes a detailed description of the experimental procedures and the statistical analysis performed.

3. The third part of the document presents the results of the study, including a comparison of the different methods and techniques used. It also discusses the implications of the findings and the potential applications of the research.

4. The fourth part of the document provides a conclusion and a summary of the key findings. It also includes a list of references and a list of figures and tables.



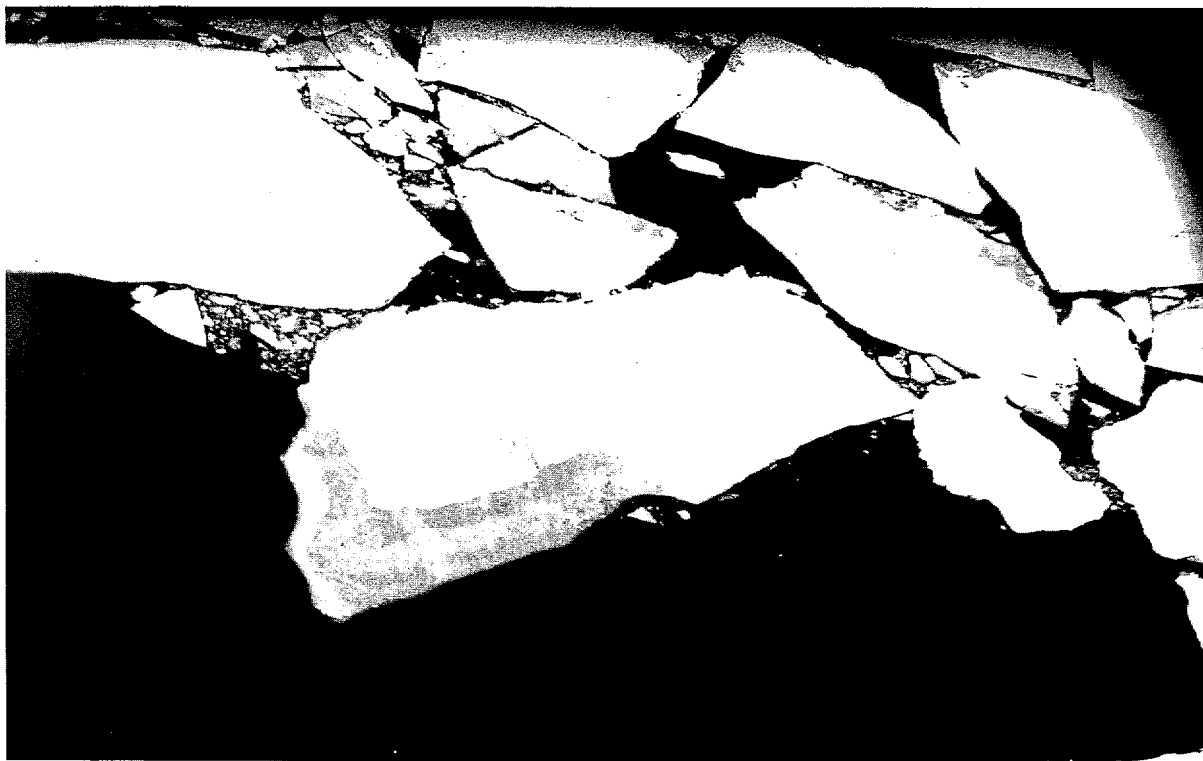
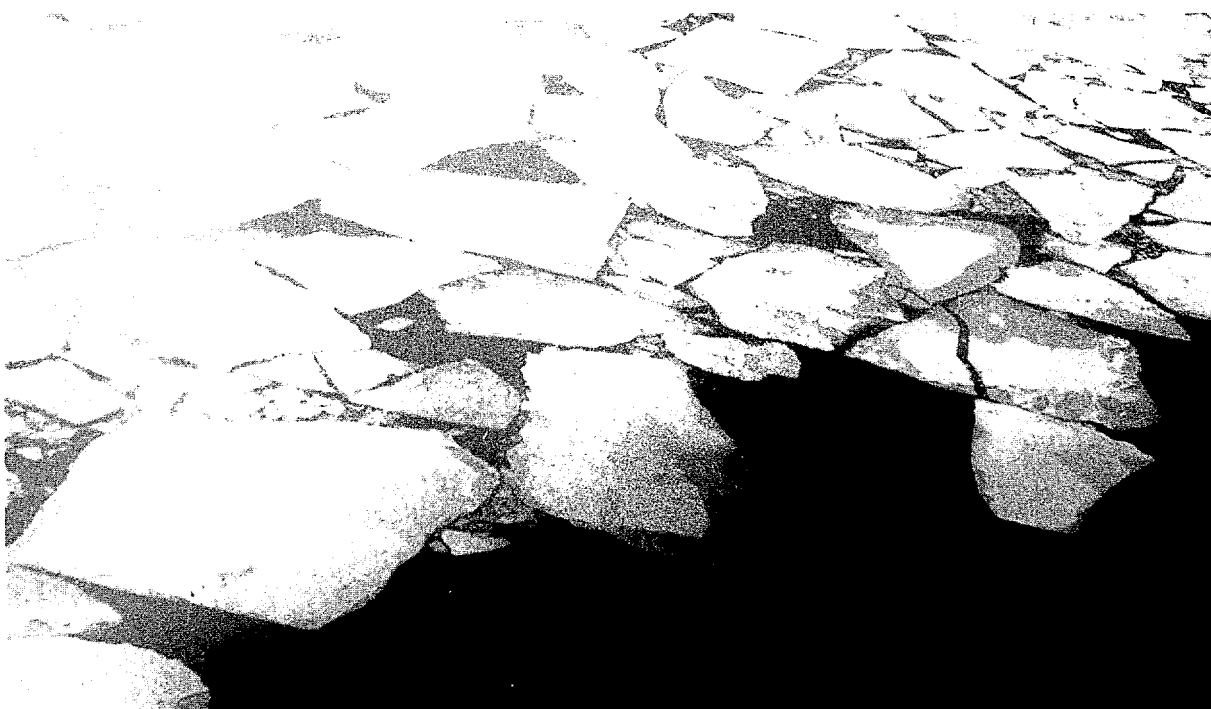


Figure 1a, b. Aerial photographs of the floe: (a) The floe and its surroundings, (b) a close-up view.

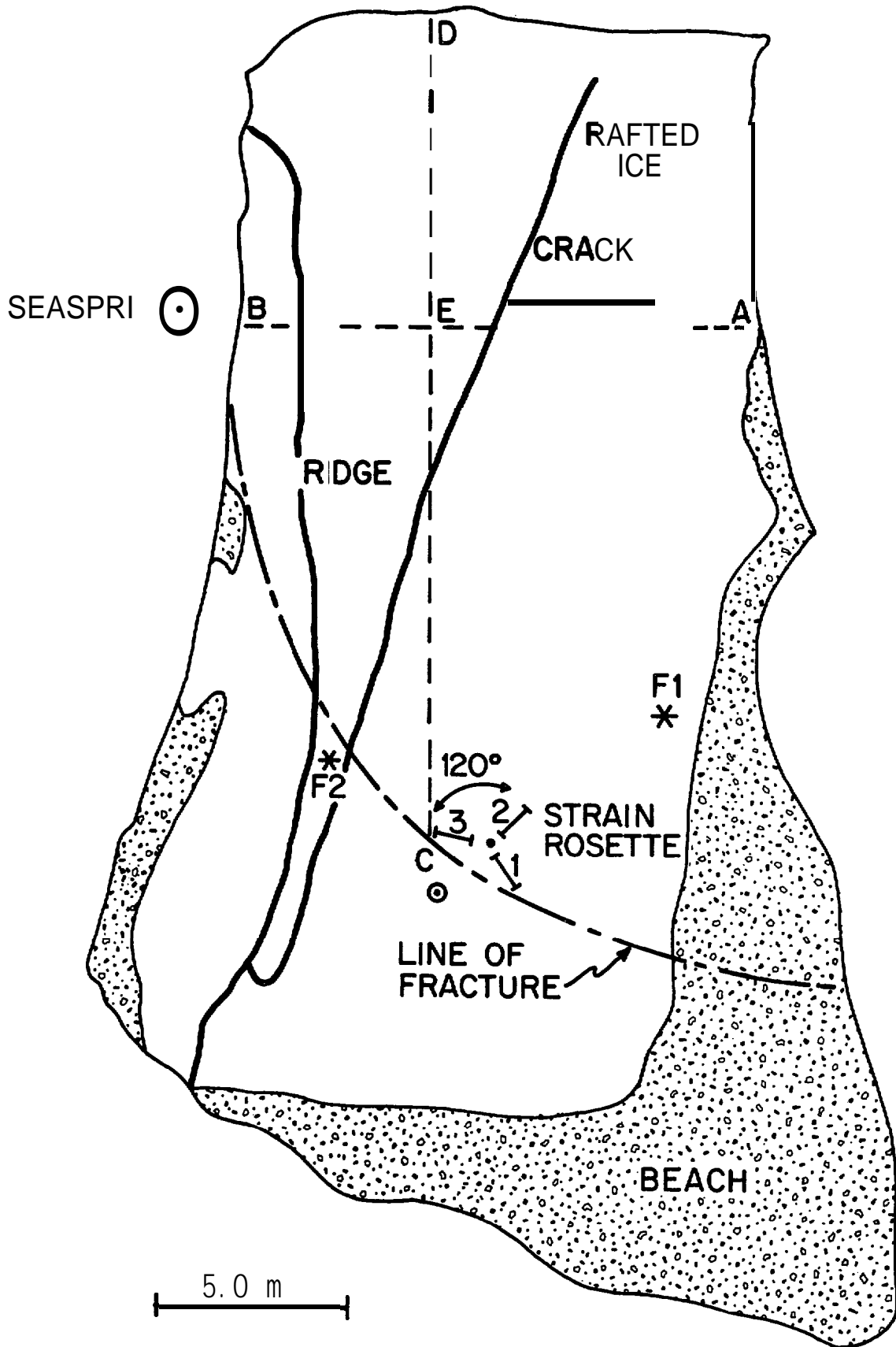


Figure 2. A map of the floe. F1 and F2 mark the core hole positions; dashed lines BEA, DEC show approximate positions of underwater surveys.

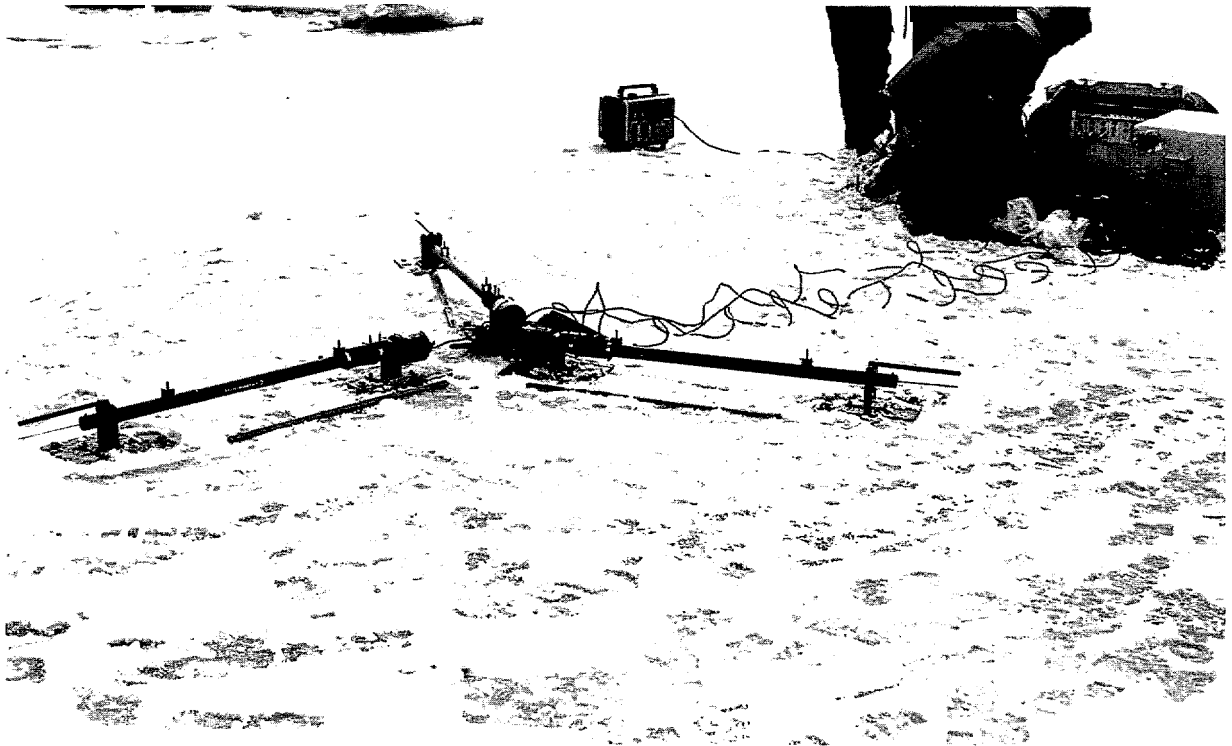


Figure 3a, b. Surface photographs: (a) Looking down the ridge;
(b) the strain rosette.

Figure 4 shows the temperature, salinity, and crystal structure of each core; F1 was 280 mm long, and F2 was 300 mm long, where Figure 2 shows the core locations. Similarly, Figure 5 shows photographs of these cores. The core F1 consisted of a mixture of frazil and columnar ice, with a 145 mm thick layer of frazil ice at the top over a mixture of columnar and frazil. The snow had the highest observed salinity of 18 ‰; the ice core had an average salinity of 8.2 ‰ and an average temperature of -3.7°C. The second core had a 175 mm thick layer of columnar ice over a 125 mm thick layer of frazil ice which suggests that the pieces of the floe on either side of the crack may have formed under different conditions. This core had an average salinity of 7.6 ‰ and an average temperature of -3.4°C.

Finally, divers from the ship investigated the under-ice topography after the floe had fractured. They did this by running knotted lines beneath the floe, then recording the ice depth at each knot from their wrist pressure gauges at 10 foot intervals along the line. Figure 6 shows the results of the traverses; beneath the small pressure ridge the ice reached a depth of 3.5 m. The amount of material piled beneath the ice is in great contrast with the smooth appearance of the surface; this result is consistent with our striking but not recovering deep rafts with the SIPRE corer. In summary, the floe consisted of a smooth 0.3 m thick ice sheet over a highly irregular bottom topography.

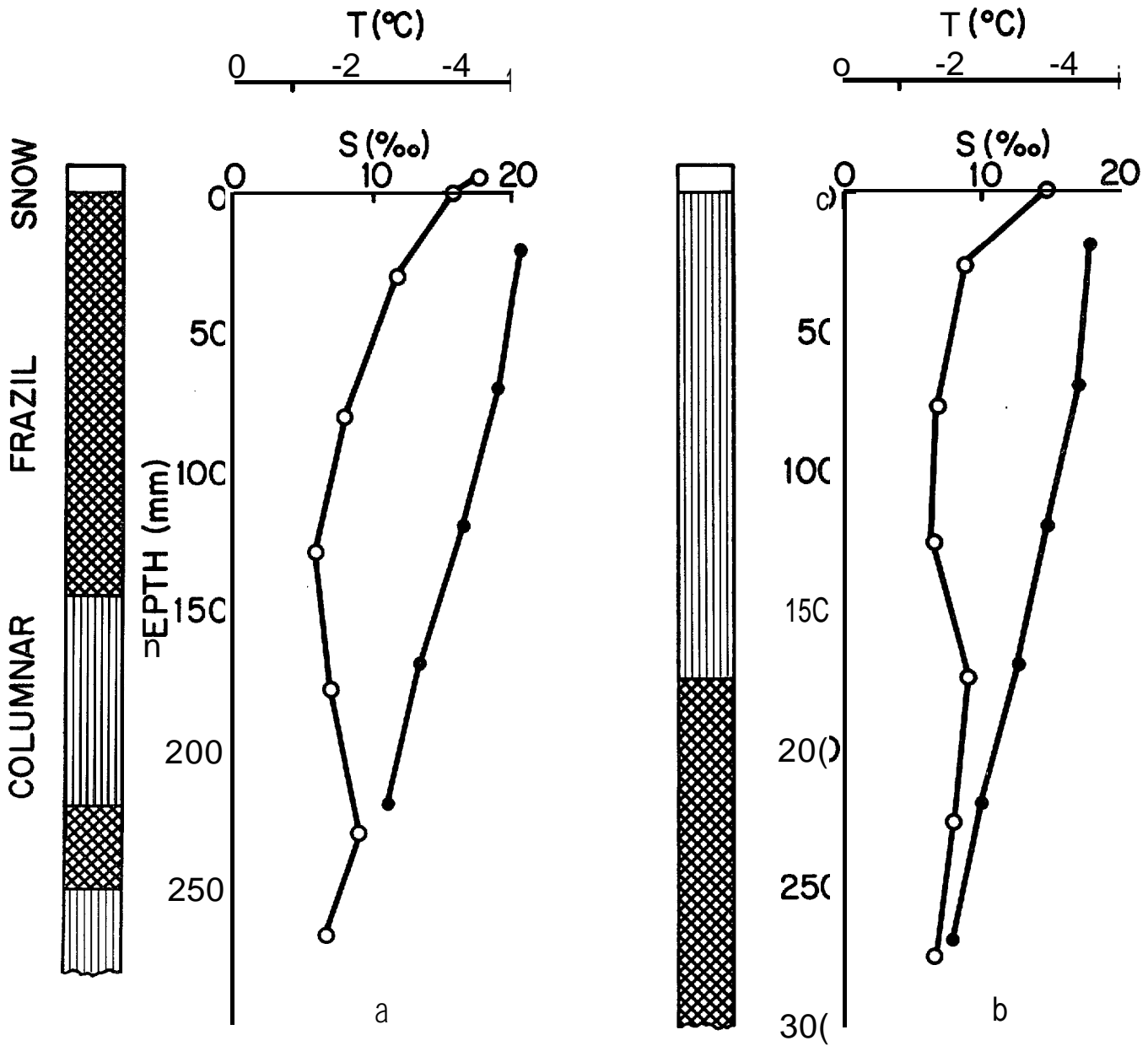


Figure 4a, b. Salinity (o), temperature (o), and crystal structure of the ice cores versus depth (a) F1, (b) F2.

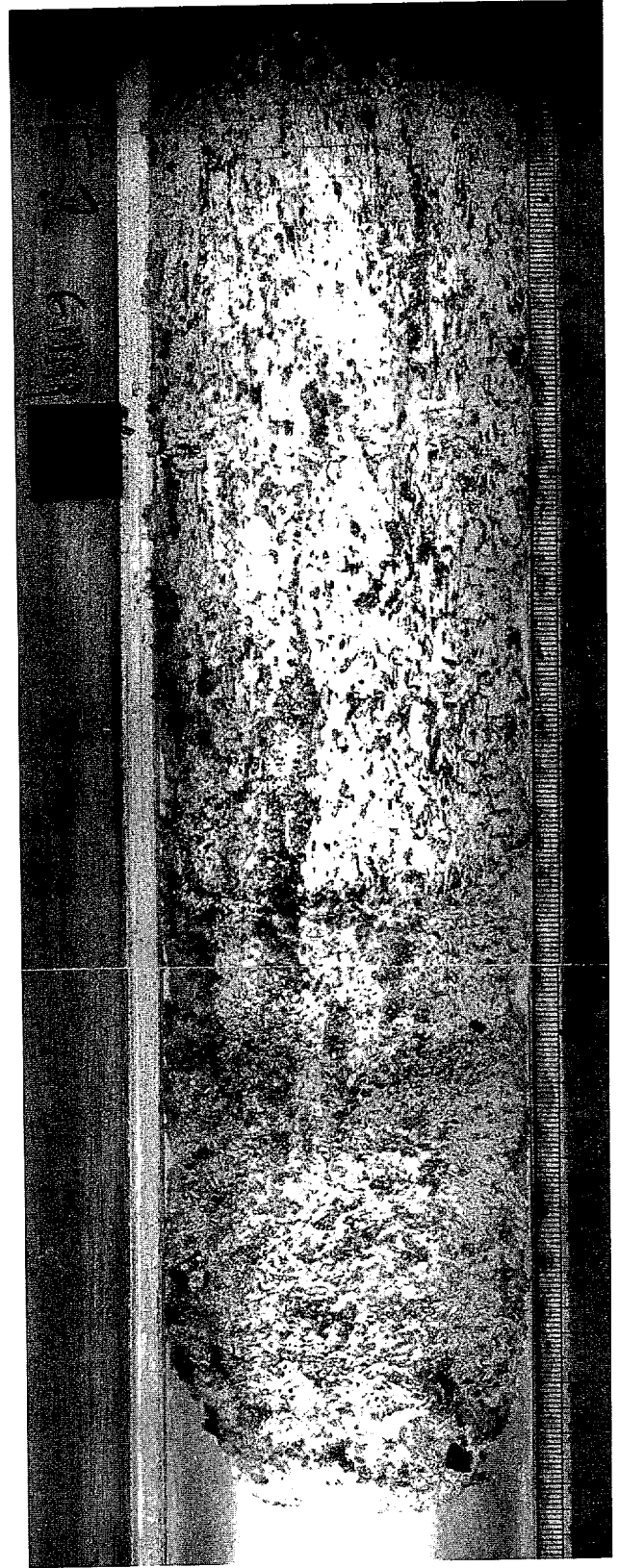
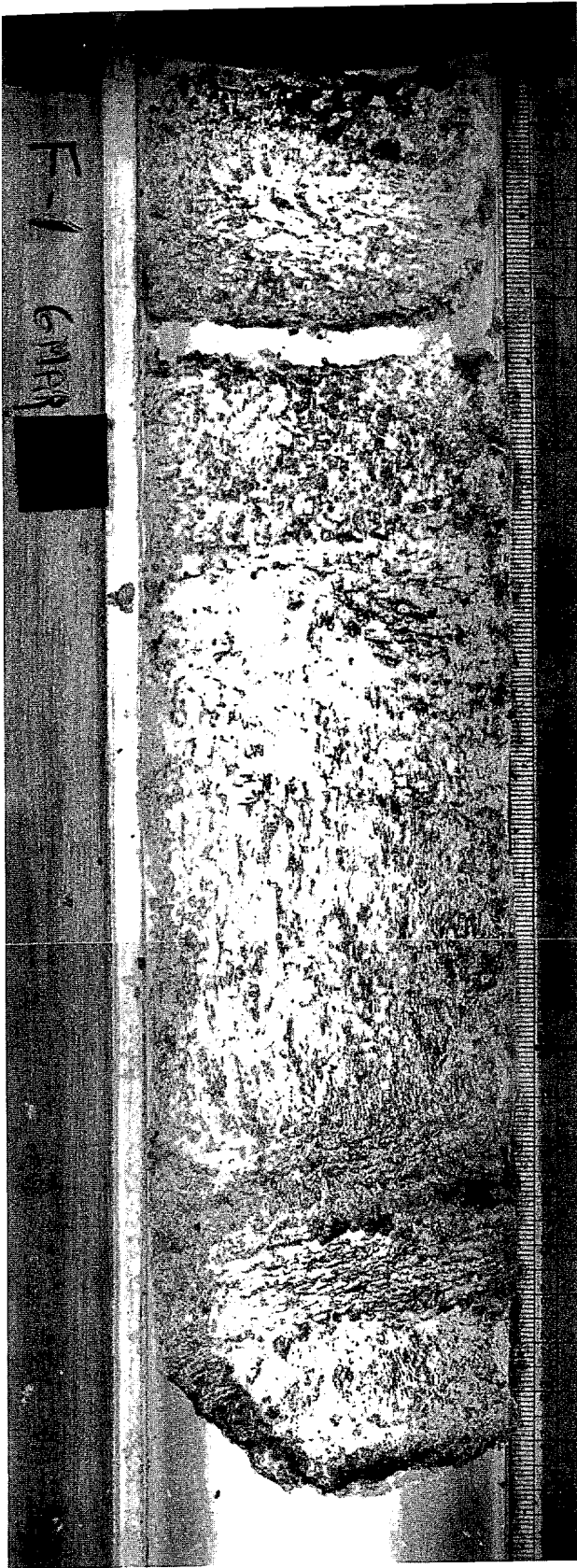


Figure 5. The core photographs: F1, F2; core top is at page top.

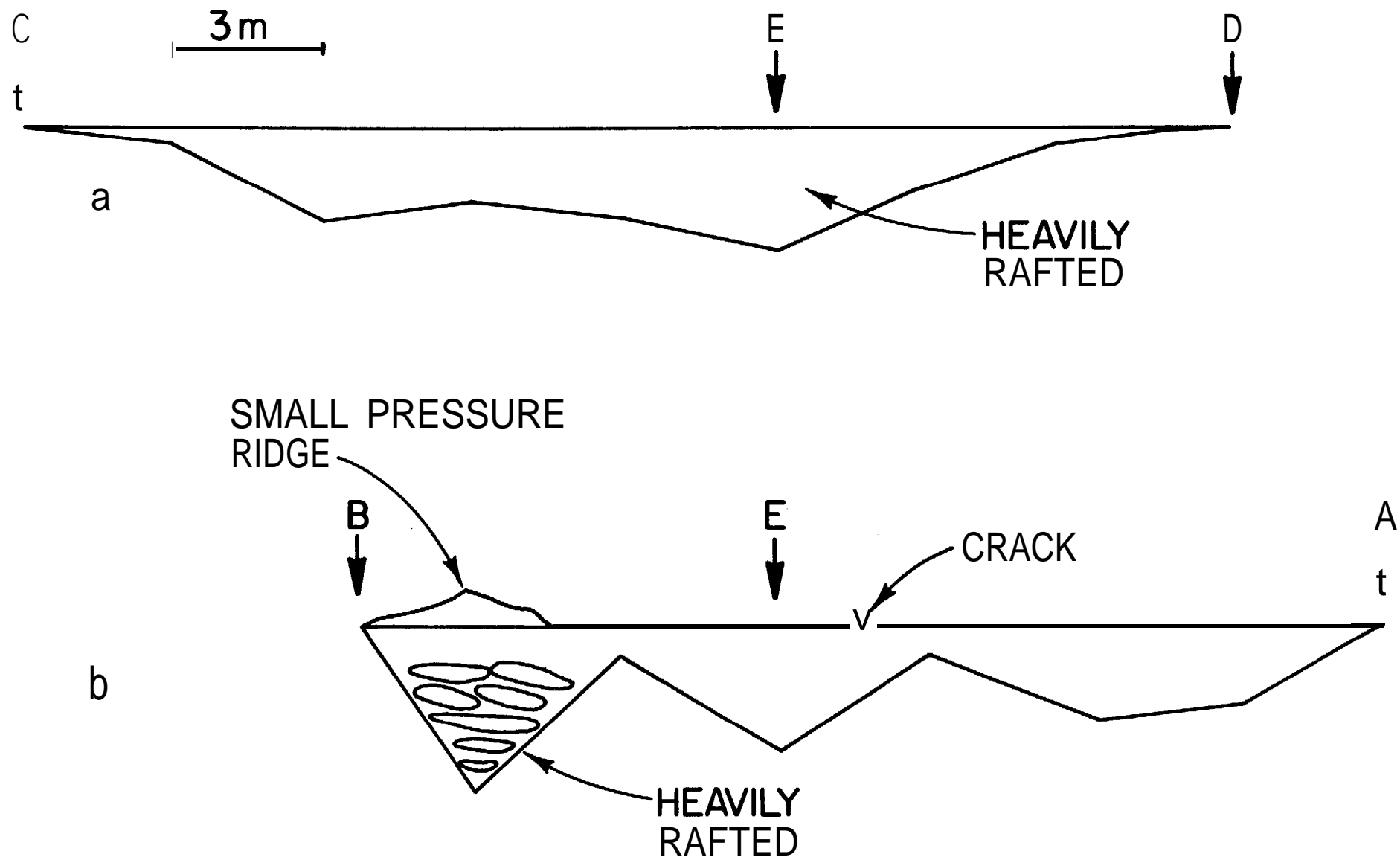


Figure 6a, b. The underwater traverses: (a) Line CED, (b) line BEA.

INSTRUMENTS

Strainmeters

The rod **strainmeters** and the associated electronics used throughout the experiment were developed by SPRI and the **Cavendish** Laboratory at Cambridge University from an earlier design for a geophysical wire **strainmeter** (King and **Bilham**, 1973). The active unit in the instrument is an **LVDT** (Linear variable differential transformer) with its core fixed directly to a 1 m **Invar** rod. When strain occurs, the rod moves the core within the transducer body. The resulting change in signal is then amplified and recorded either digitally after filtering at the **Nyquist** frequency, or with an analog FM tape recorder. The output may also be monitored using a standard chart recorder. Should the measured signal drift off-scale, it is returned to zero using a small motor to drive the entire transducer assembly horizontally on bearings independent **of the** core. To avoid lateral movement of the core within the LVDT, the core is mounted between two rosettes of steel springs. At the other end of the strainmeter the **Invar** rod is clamped rigidly to the base unit. A clamping bar links the two ends for transportation and facilitates easy deployment on the ice where standard 6 inch coach screws are used to bond the instrument securely to the **floe** surface.

Accelerometers

The sea state local to the ice floes was measured using a vertically mounted Schaevitz-EM servo accelerometer housed within the waterproof cap of a free-flooding, vertical spar buoy with chain ballast (**SEASPRI**) (**Wadhams** and Squire, 1980). A single accelerometer introduces an error due to sea surface tilt but for the wave periods encountered, it is found to be < 1%.

The vertical bodily accelerations of the floes were measured **by** a similar accelerometer in an environmental housing placed directly on the ice surface. Again the error introduced by tilt is negligible. The two acceleration records allow **us** to determine the heave response of ice floes over the range of frequencies present in the open sea.

During the experiments we also deployed a Waverider buoy from the SURVEYOR to measure sea state. The instrument is a freely floating sphere containing a gimbal-mounted accelerometer which integrates measured acceleration to give sea surface displacement. The data are then transmitted back to a data logger where they are filtered and recorded at a sampling rate of half a second. The buoy could easily be deployed and retrieved using the telescoping boom crane on the forecastle of the ship.



DATA ANALYSIS

The basic hypothesis behind any data analysis performed on ocean wave data is that the sea surface may be regarded as a random process. **Furthermore**, the process is assumed to be statistically stationary and **ergodic** (Bendat and Piersol, 1971); otherwise little progress can be made. With these assumptions it is possible to define a Power Spectral Density (PSD) function $G(f)$ which may be used to relate energy density with frequency f . This may be generated as follows: Consider a stationary and **ergodic** random process $y(t)$. It is not possible to define a Fourier transform[*] in the usual way, viz.

$$Y\{Y(t)\} = \int_{-\infty}^{\infty} y(t) e^{-i2\pi ft} dt, \quad (1)$$

since such a process cannot satisfy absolute **integrability**. It is also true, however, that $y(t)$ is impossible to measure since it requires a knowledge of y for all time t . Consider instead a sample

$$y_T(t) = \begin{cases} y(t), & -\frac{T}{2} \leq t \leq \frac{T}{2} \\ 0 & |t| > \frac{T}{2} \end{cases} \quad (2)$$

For this function a Fourier transform can be defined and will exist for all $T < \infty$. We may then apply Parseval's theorem (Lathi, 1965) to obtain

$$\int_{-\infty}^{\infty} |y_T(t)|^2 dt = \int_{-\infty}^{\infty} |Y\{y_T(t)\}|^2 df. \quad (3)$$

We cannot allow $T \rightarrow \infty$ since the Fourier transforms which we denote as $Y\{\cdot\}$, is then undefined. However, the expected **value** of $|Y\{y_T(t)\}|^2$ does exist,

so that

$$\overline{Y^2} = \int_{-\infty}^{\infty} \text{Limit}_{T \rightarrow \infty} \frac{E[|Y\{y_T(t)\}|^2]df}{T} \quad (4)$$

The integrand in this expression is called the two-sided PSD. If we restrict frequency to positive values, then we may define the more usual one-sided PSD as

$$G(f) = 2 \text{Limit}_{T \rightarrow \infty} \left\{ \frac{E[|Y\{y_T(t)\}|^2]}{T} \right\}, \quad (5)$$

so that

$$\overline{Y^2} = \int_0^{\infty} G(f)df, \quad (6)$$

From this equation it can be seen that the mean-square-value of sea surface displacement can be found by integration of the PSD over frequency space. Likewise, the mean-square-value of wave displacement at particular frequencies may be found by integration over small frequency bandwidths.

The PSD may be characterized statistically by its moments. We define the n^{th} moment of the spectrum by

$$m_n = \int_0^{\infty} G(f) f^n df, \quad (7)$$

(Pitt *et al.*, 1978) so that the zeroth moment may be interpreted as the mean-square sea elevation $\overline{y^2}$ or equivalently, the total energy in the wave system. From the moments a set of parameters have evolved which are of interest in oceanographic and ocean engineering applications. We define only those parameters used in the current text:

$$\text{Significant wave height, } H_s = 4\sqrt{m_0},$$

$$\text{Mean zero crossing period, } T_z = \sqrt{\frac{m_0}{m_2}} \quad ,$$

$$\text{Goda's spectral peakedness parameter, } Q_p = \frac{2 \int_0^{\infty} f G^2(\alpha) df}{m_0^2} \quad ,$$

(Goda, 1970). For a more comprehensive list of currently used wave parameters, many of which were developed for **nonspectral** analysis, see for example Pitt *et al.* (1978).

The actual mechanics involved in producing a power spectrum have been considerably simplified with the introduction of the FFT (Fast Fourier Transform) algorithm of Cooley and Tukey (1965). This algorithm computes the Fourier transform $Y\{\cdot\}$ of the time series $y(t)$ by decomposing its $N (= 2^p)$ where p is an integer) digitized points into composite (nonunity) factors and then transforming over the small number of terms in each factor. From $Y\{\cdot\}$, using equation (5), an estimate PSD for a single sample may then be found from

$$G(f) = \frac{2}{T} |Y\{y(t)\}|^2 \quad . \quad (8)$$

Unfortunately, such an estimate PSD has a standard error of unity (Wadhams, 1973) so that some averaging must be carried out. Frequency **smoothing**, whereby a single sample record is used and contiguous spectral components are averaged, is used in the current work. Neglecting bias errors, the standard error when this type of smoothing is carried out is

$$\frac{1}{\sqrt{\text{Grouping factor}}} \quad ,$$

where the grouping factor is the number of frequency components used.

For the Bering Sea cruise data the original time series were filtered at 1 s to avoid **aliasing**, and either digitized manually or through the PDP-11 coupled A-D facility at Cambridge University. The digitized records were then processed to remove **rezero** steps using an interactive routine developed by the Sea Ice Group at SPRI (Ray Home, personal communication, 1979). These rezero steps had either been introduced into the data by the servo motor in the rod **strainmeters**, or manually in the case of the accelerometers. The mean and trend were then removed, and the end tenths of each time series tapered to reduce side lobe leakage (Bingham *et al.*, 1967). Finally, the SPRI FFT/graphics package was run on each record with a grouping factor of nine. The standard error in all the smoothed spectra is therefore one third.

THE BERING SEA DATA AND THEIR INTERPRETATION

Seastate

The Waverider and SEASPRI buoys were used in the open water to monitor the incident wave energy during the experiment. Both instruments can provide an estimate of sea surface displacement at a particular location though the directionality of the propagating ocean waves and their spread cannot be found. Stereo mapping techniques, several wave probes, or a buoy which is able to measure tilt as well as elevation, are necessary for a complete picture (Kinsman, 1965). Such an experiment would be virtually impossible to carry out near a marginal ice zone so that we are necessarily limited to a nondirectional analysis.

Unlike the Waverider buoy, SEASPRI has no integrating circuits in the electronics so that the recorded time series represents the sea surface acceleration in m s^{-2} rather than displacement. The record may be corrected to displacement by first assuming that the sea surface is composed of the sum of an infinity of sinusoids of random phase. Then, for the n^{th} component mode

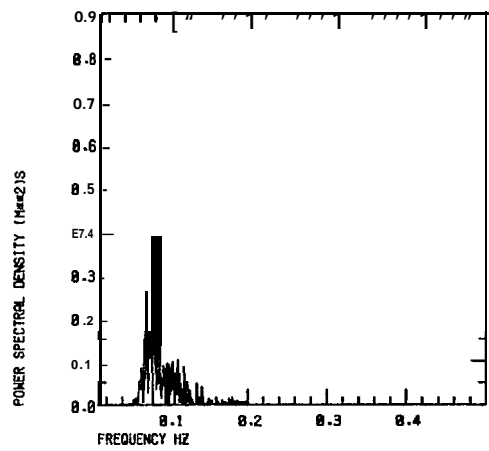
$$Y_n = A_n \cos \left(\frac{x}{\lambda_n} - f_n t + \alpha_n \right), \quad (9)$$

the acceleration is given by $4\pi^2 f_n^2 y_n$, where y_n is displacement, A_n is amplitude, λ_n is the wavelength, f_n is the frequency and α_n is the phase. It is clear that in principle, correction from acceleration to displacement is simple and merely involves division by $4\pi^2 f_n^2$. For a real sea where an infinity of modes exist, this computation must take place in frequency space so that it is not possible to generate a SEASPRI displacement time series directly. Working with the SEASPRI record then, we see that to convert to the usual

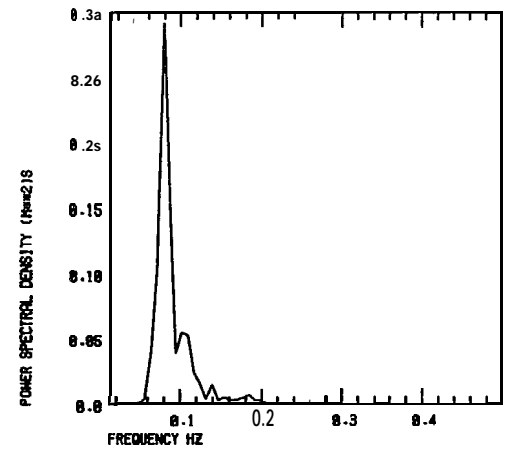
power spectrum representing ocean wave energy, we must divide each spectral component by $16\pi^4 f^4$. When this operation has been carried out, the spectra from the two buoys should be equivalent. In reality, the two sets of spectra are somewhat different. This may be attributed to three factors: The respective time **series** are not simultaneous and were recorded about a kilometer apart, the record lengths and hence the frequency combs for the spectra are different (SEASPRI records were 30 minutes in length whereas the **Waverider** records were only 20 minutes), and there was a tendency for the SEASPRI buoy to move with the floe so that its high frequency response was impeded. Typically, a comparison between the two wave buoys gives significant wave heights which differ by only 0.04 m and spectral peakedness parameters which differ by 0.4. The worst discrepancy is in the statistical wave periods where the estimates from SEASPRI can be as much as 2.5 s higher than the equivalent Waverider buoy period. Clearly SEASPRI is moving with the floe. Power spectra from each of the buoys are shown in Figure 7 where the **ungrouped** and grouped spectra, and the original time series are shown. Figures 7a, b, c, and d represent Waverider buoy data, and Figures 7e, f, g, and h represent the SEASPRI data. The grouped spectra bear a remarkable similarity for all but the low period energy, indicating that our interpretation in terms of statistical parameters may have been overly pessimistic. We shall therefore regard the **SEASPRI** data as a measure of the forcing in our experiment and "normalize" all our records from simultaneously-recording, floe-mounted instruments with respect to the SEASPRI spectra. The low period energy apparent in the power spectra, however, will be treated with caution.

A further question we may pose before leaving our discussion of the open water wave energy concerns our original assumption of **stationarity**.

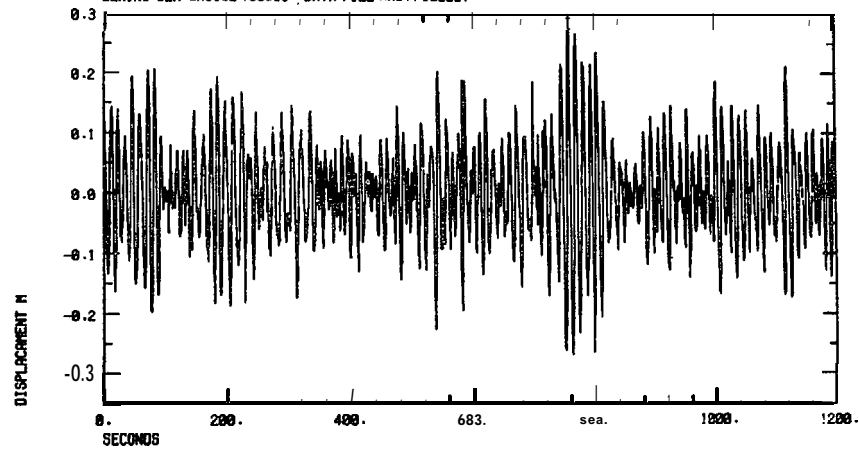
BERING SEA CRUISE 7993S6 . DATA FILE WRB(FILE22).
 GROUPING FACTOR= 1
 RECORD LENGTH= 1200.0



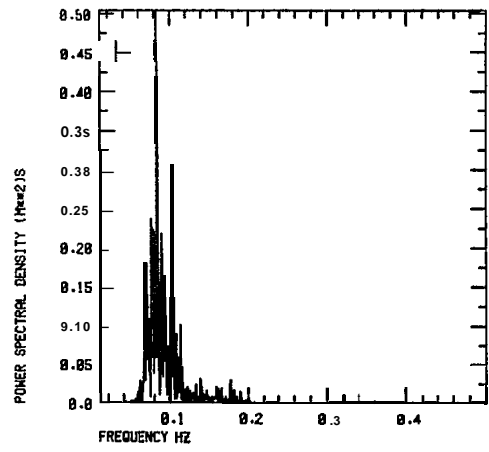
BERING SEA CRUISE 790306 . DATA FILE NRS(FILE221).
 GROUPING FACTOR= 9
 RECORD LENGTH= 1200.0



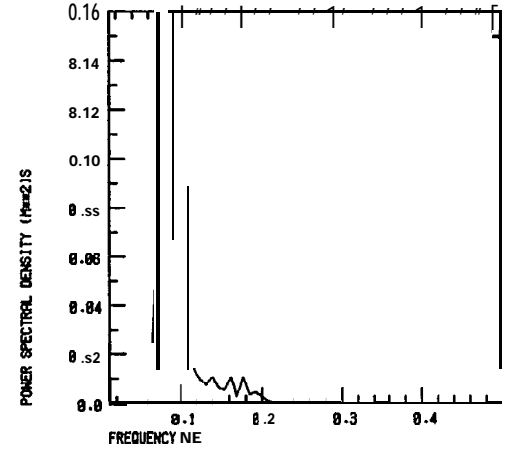
BERING SEA CRUISE 790306 . DATA FILE WRB(FILE22).



BERING SEA CRUISE 790306 . DATA FILE WRB(FILE22).
 GROUPING FACTOR= 1
 RECORD LENGTH= 1200.0



BERING SEA CRUISE 790306 . DATA FILE WRB(FILE22).
 GROUPING FACTOR= 9
 RECORD LENGTH= 1200.0



BERING SEA CRUISE 7S82SS . DATA FILE WRB(FILE22).

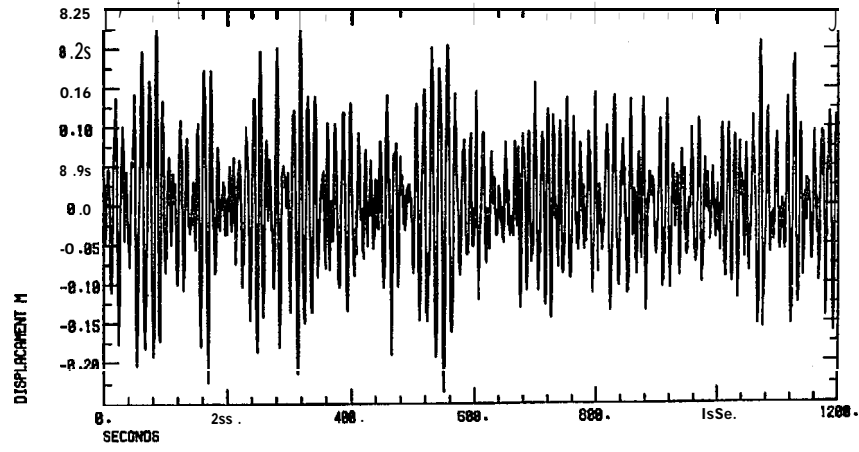


Figure 7a, b. Time series and power spectra for two 20 minute Waverider buoy records. Records begin at 10.30 and 10.50 respectively.

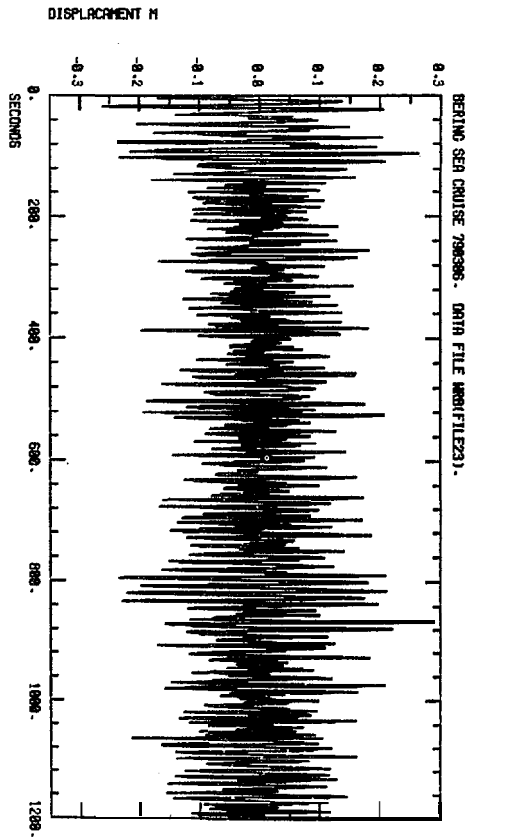
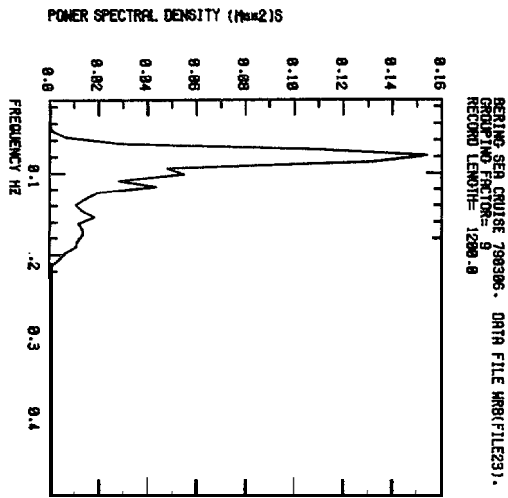
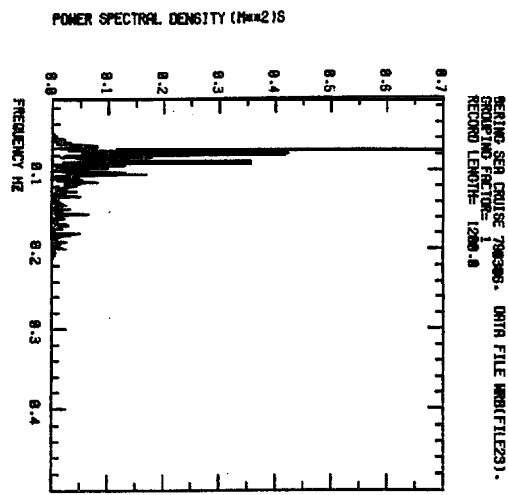
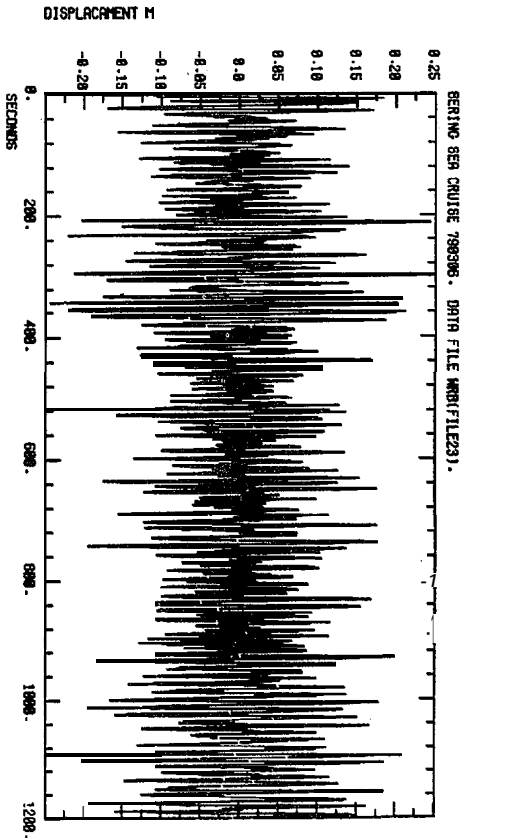
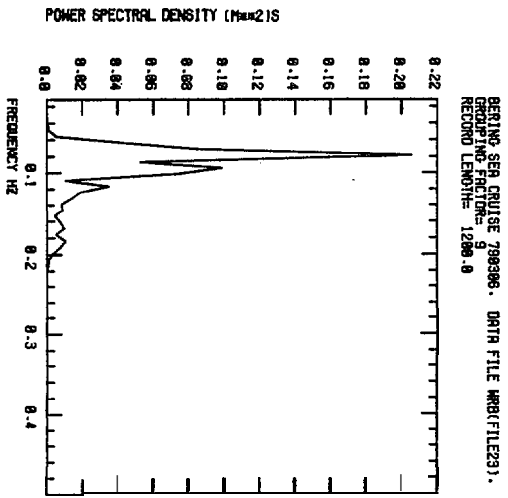
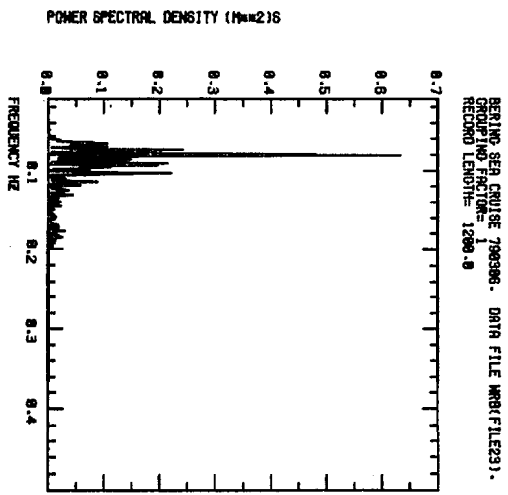


Figure 7c, d. Time series and power spectra for two 20 minute Waverider buoy records. Records begin at 11.12 and 11.32 respectively.

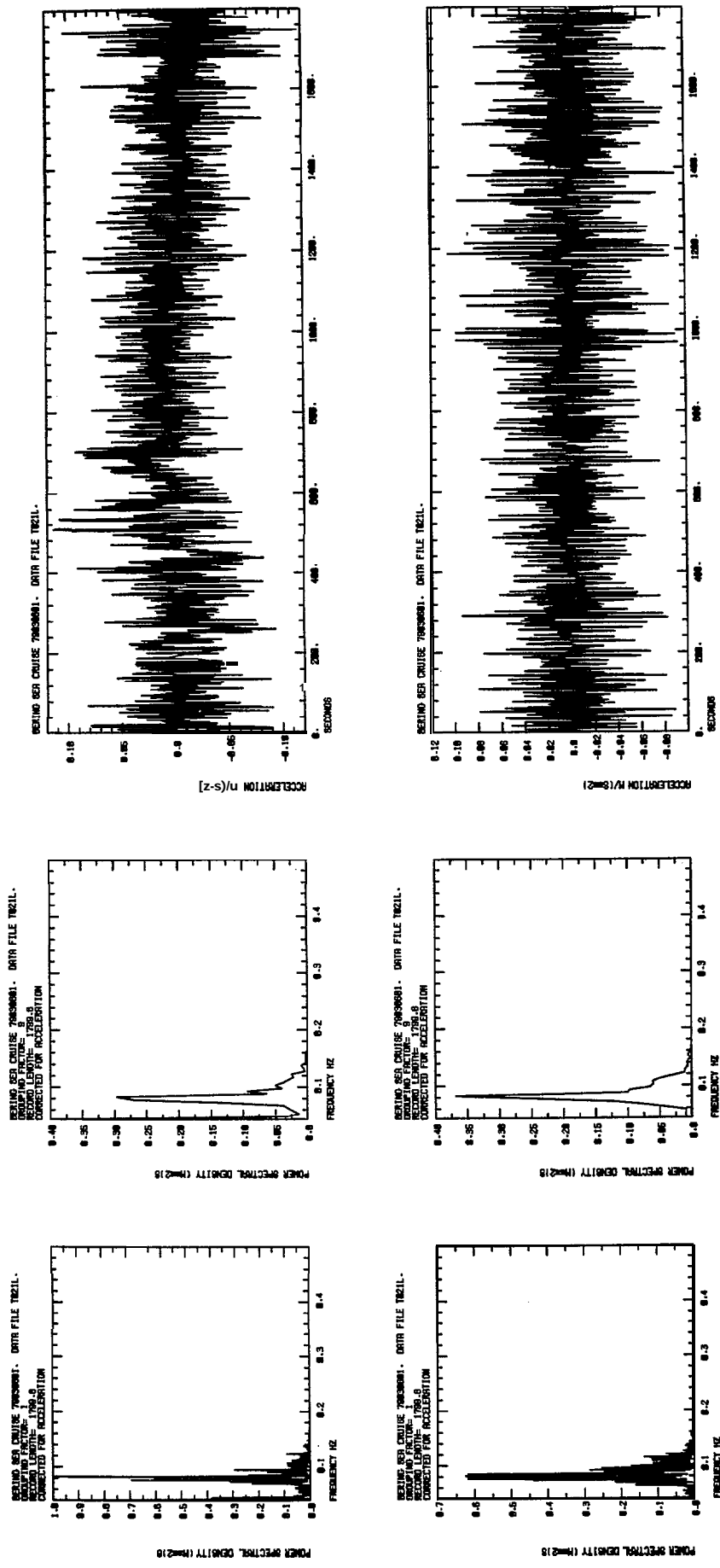
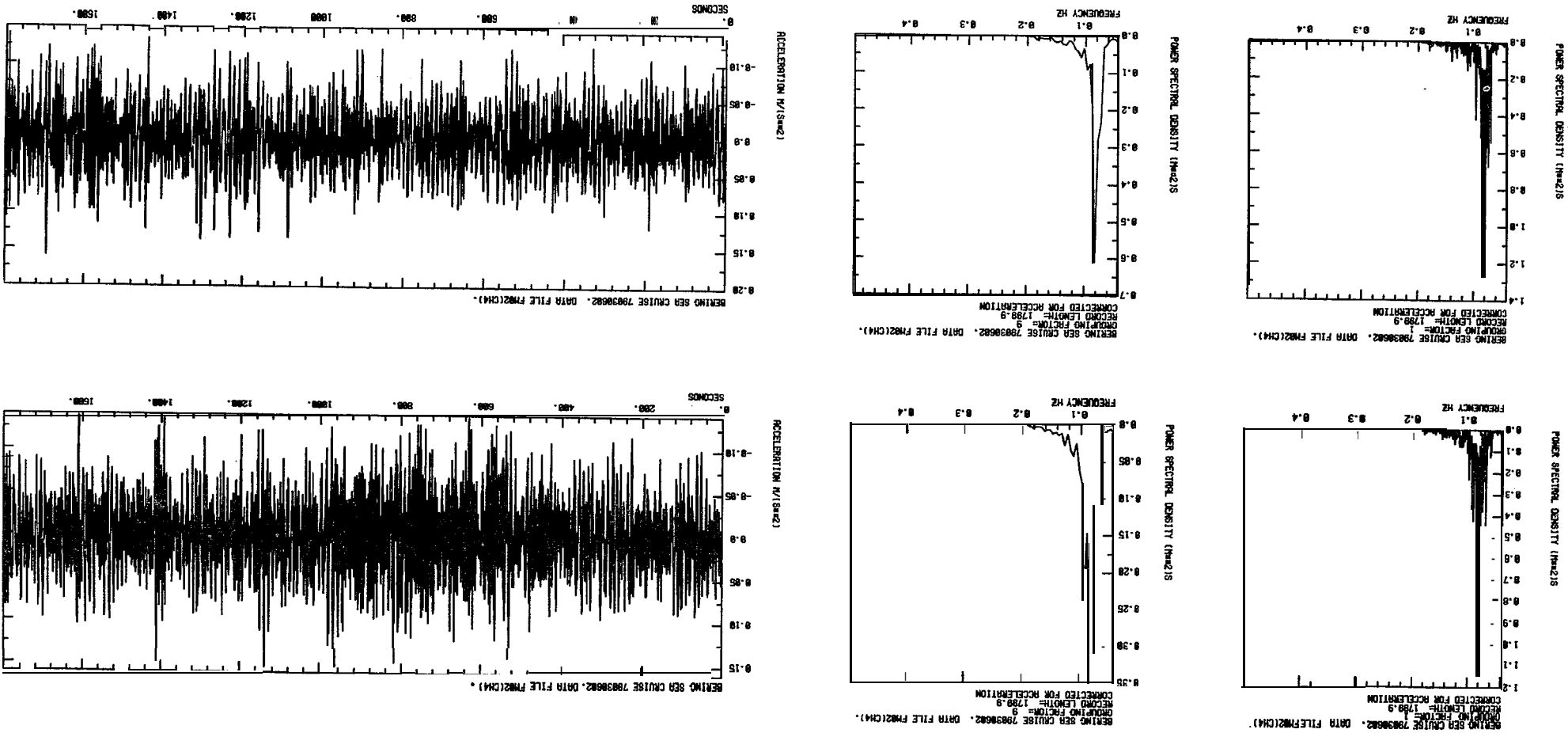


Figure 7e, f. SEASPRI time series and power spectra for two 30 minute records beginning at 10.38 and 11.08 respectively.

Figure 7g, h. SEASPRI time series and power spectra for two 30 minute records beginning at 11.56 and 12.26 respectively.



We have four contiguous records from the Waverider buoy so within the duration of the experiment, we may compare the statistical parameters from consecutive power spectra (Table 1).

Table 1. Comparison of statistics for consecutive Waverider buoy spectra.

	<u>Record 1</u>	2	3	4
Significant wave height, m	0.32	0.29	0.29	0.30
Mean zero crossing period, s	9.9	10.0	9.3	8.7
Spectral peakedness	3.9	3.2	3.1	2.5

The data show a general spectral broadening with negligible change in significant wave height. The peak representing swell in the 12-13 band is stationary while there is a noticeable buildup of energy between 5 and 6 s. This increase in low period energy leads to a shortening of the mean **zero**-crossing period and the decrease in the spectral peakedness (a high Q_p implies a narrow spectrum). We see once again, therefore, that we must proceed with care in our interpretation of the data at shorter periods.

An additional observation which we mention only in passing since it preempts subsequent data analysis, is that within an hour or so of our leaving the floe, it cracked into two parts. If we assume that this fracture was due to wave-induced **flexure**, perhaps there is a link between fracture and the onset of shorter period **waves** of significant amplitude. This may be argued qualitatively if the floe is assumed to bend perfectly **to** the sea surface. Then a short wave will cause large curvature whereas for the longer waves, the floe will tend to ride the wave and bend less.

Heave Response

The heave response of **our floe** may be computed from the floe-mounted accelerometer data. This accelerometer was placed close to the strainmeter rosette approximately 10 m from the SEASPRI buoy (Figure 2). The recorded time series are synchronized with the equivalent SEASPRI wave record, and are of the same duration. Figures 8a, b, c, and d show the **ungrouped** and grouped power spectra, and the time series generated in the same way as for the SEASPRI data. The spectra have again been **adjusted by** division by a factor $16\pi^4 f^4$ so that the integrated value of PSD over frequency space represents the mean square amplitude of heave. This enables a direct comparison to be made between the floe-mounted accelerometer and the corresponding SEASPRI spectra.

The grouped spectra show the same spectral peak between 12 and 13 s but do not show the short period energy characteristic of the Waverider buoy spectra. This is to be expected since **one would** think that most of the short period energy would be reflected (Wadhams, 1973). The resonant heave frequency (Lee, 1976) of the ice floe in this case is so close to the spectral peak, and the incident wave forcing spectrum is so narrow, that no discernible natural oscillation can be isolated. The significant wave height, which may be interpreted as the significant height of heaving, is approximately 0.3 m for all the records.

A direct comparison between incident wave energy (as measured by SEASPRI) and floe heave may be found by use of the frequency response function and the associated coherence function (Bendat and Piersol, 1971). The frequency response function $H(f)$ is defined:

$$H(f) = \frac{G_{12}(f)}{G_1(f)} ,$$

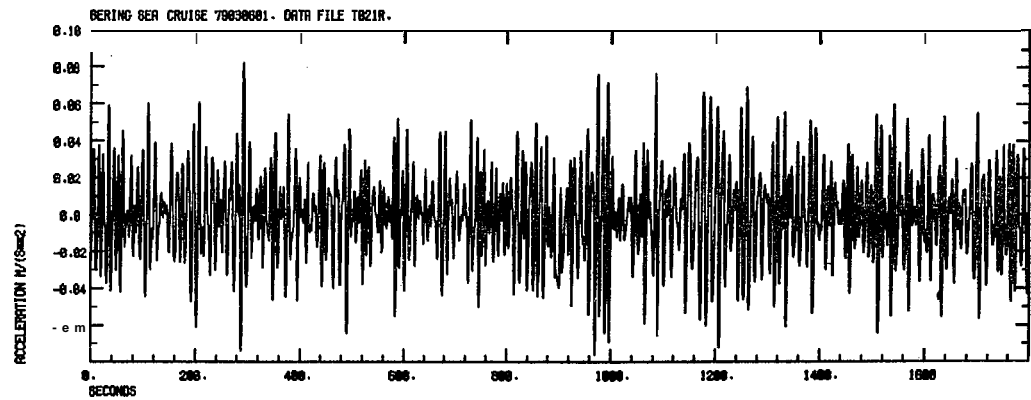
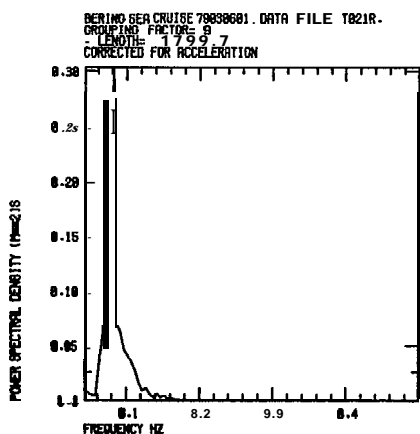
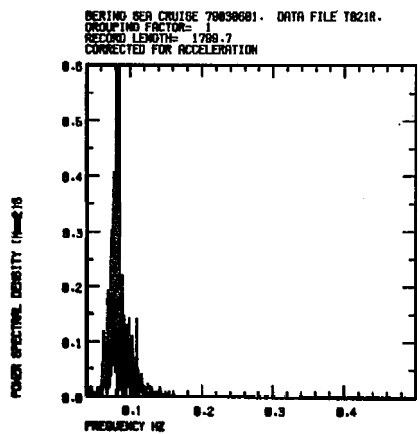
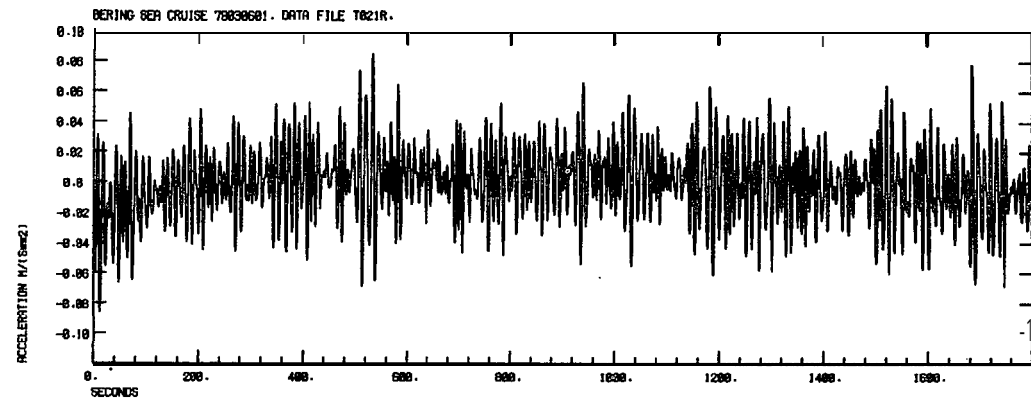
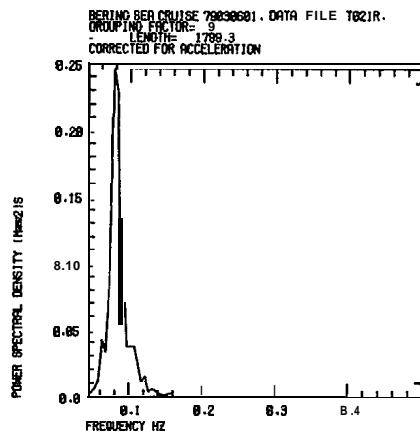
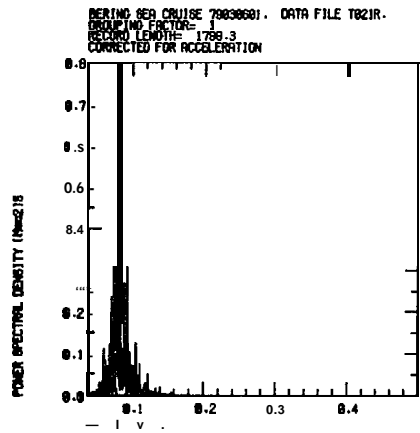
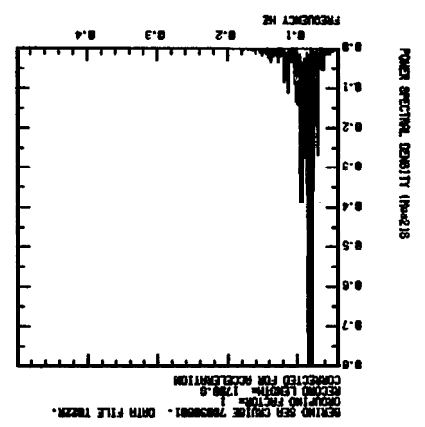
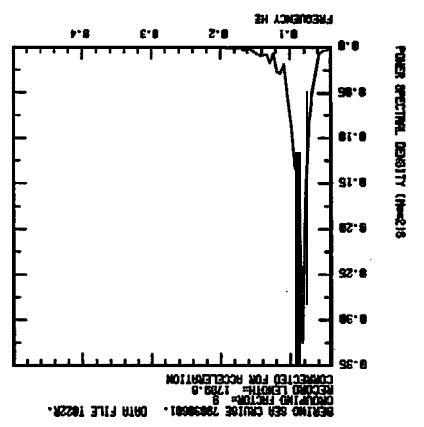
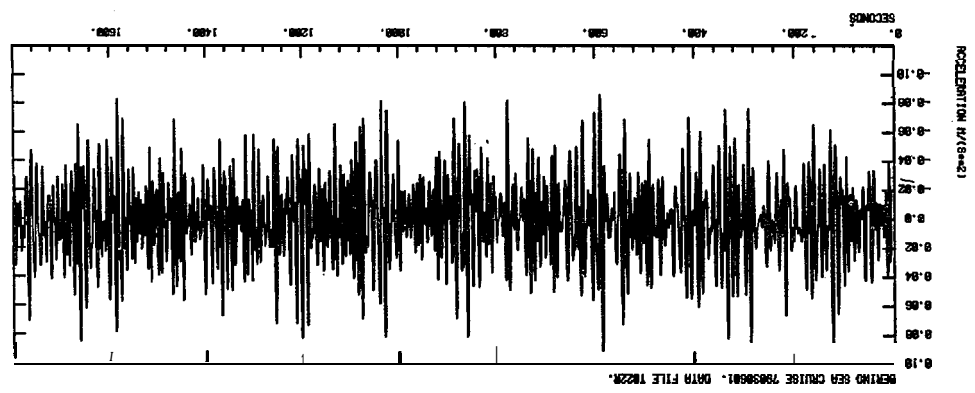
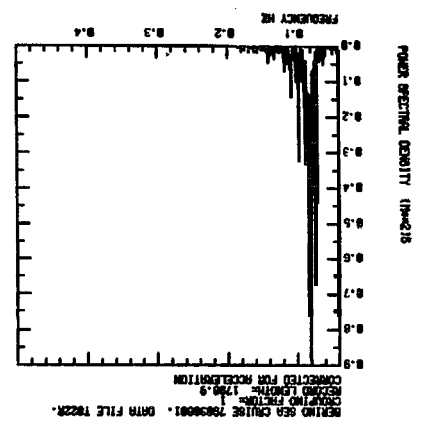
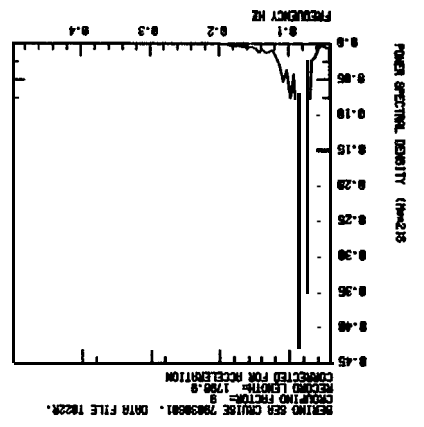
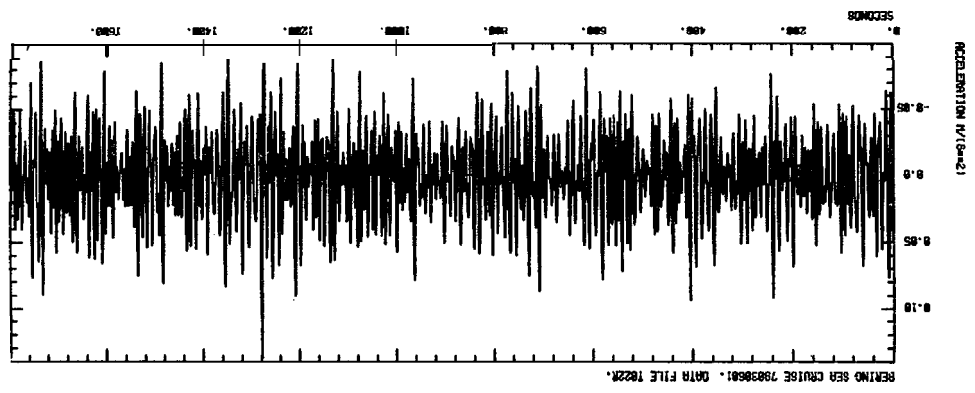


Figure 8a, b. Time series and power spectra for two 30 minute floe accelerometer records. The records are synchronized with Figure 7e, f.

Figure 8c, d. Time series and power spectra for two 30 minute floe accelerometer records. The records are synchronized with Figure 7g, h.



where G_1 is the (auto) power spectrum of record 1, and G_{12} is the cross power spectrum between records 1 and 2. The magnitude and phase of $H(f)$ are called the gain factor and phase factor, respectively. The coherence function $\gamma^2(f)$ is defined

$$\gamma^2(f) = \frac{|G_{12}(f)|^2}{G_1(f)G_2(f)} \quad (11)$$

where G_2 is the (auto) power spectrum of record 2.

In this case we consider the **SEASPRI** time series as record 1 and the floe-mounted accelerometer time series as record 2. Then the gain factor of $H(f)$ gives the floe's response as a function of frequency, and the phase factor an estimation of the phase velocity or wavelength of the propagating waves. The coherence function, which varies between 0 and 1 depending on whether the two records are completely **uncorrelated** or perfectly coherent, is used to impose confidence limits on $H(f)$ (Bendat and Piersol, 1971).

Figures 9a, b, c, and d show the frequency response function and coherence function for heave. A 95% confidence interval for the estimate has been calculated and may be used to determine a frequency domain for the gain factor within which the floe is responding "perfectly" to the incident waves. In this case the word perfectly is used loosely since the response can be anywhere within the confidence limits. In terms of period, the domain for the floe extended from about 6 to 16 s.

Interpretation of the phase factor was carried out only for those time series recorded on the same machine (Figure 9a, b). First a bathymetric chart showed that with generous bounds the water depth h beneath the floe was $45 < h < 55$ m. Then a theoretical curve was plotted for the wavelength

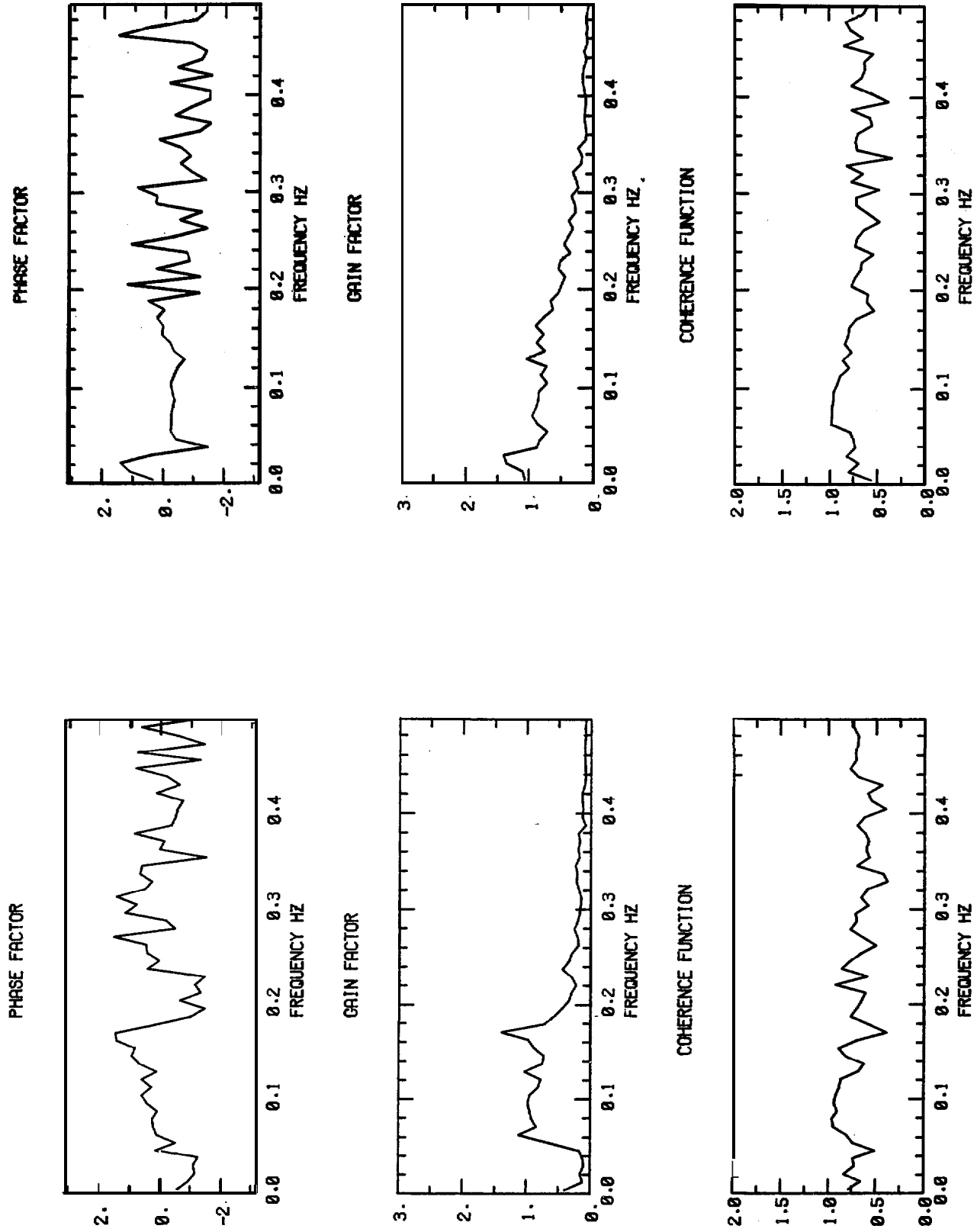
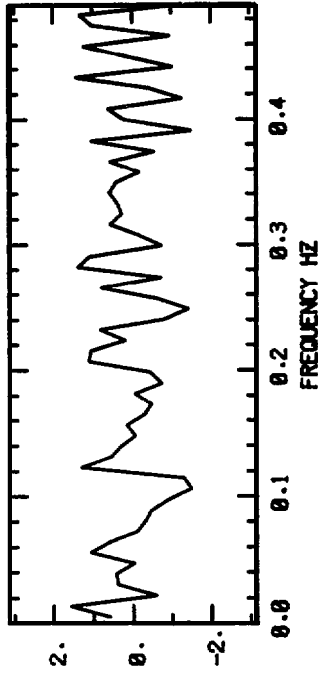


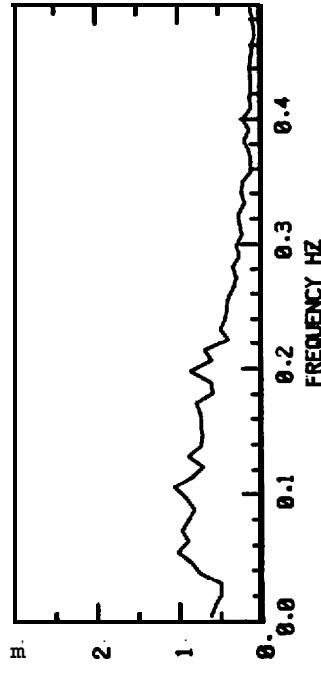
Figure 9a, b. Frequency response functions and coherence functions for floe-mounted accelerometer with reference to SEASPRI buoy,

BERING SEA CRUISE 79030602. DATA FILE FM02(CH4).
BERING SEA CRUISE 79030601. DATA FILE T022R.
GROUPING FACTOR 15

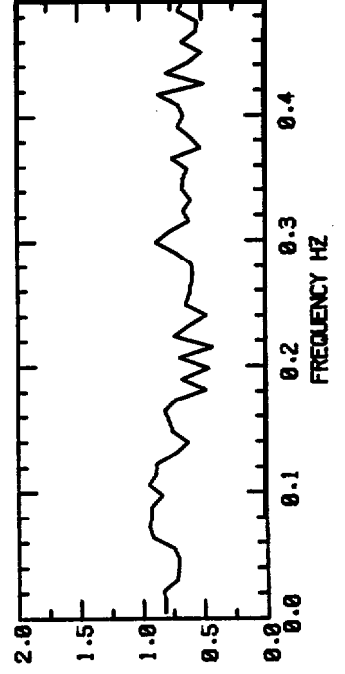
PHASE FACTOR



GAIN FACTOR

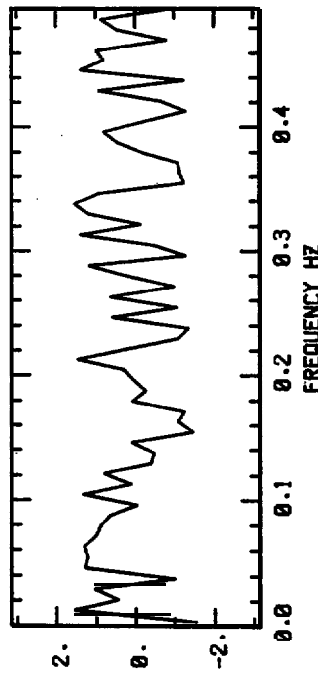


COHERENCE FUNCTION

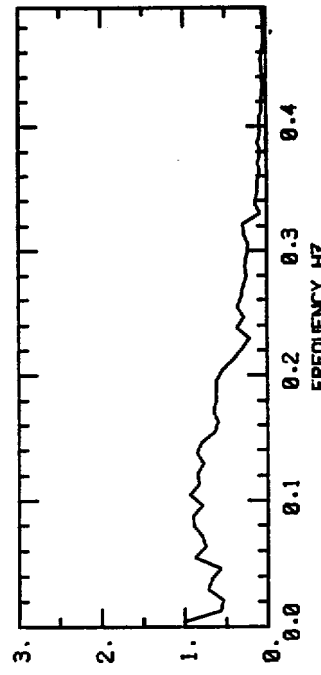


BERING SEA CRUISE 79030602. DATA FILE FM02(CH4).
BERING SEA CRUISE 79030601. DATA FILE T022R.
GROUPING FACTOR 15

PHASE FACTOR



GAIN FACTOR



COHERENCE FUNCTION

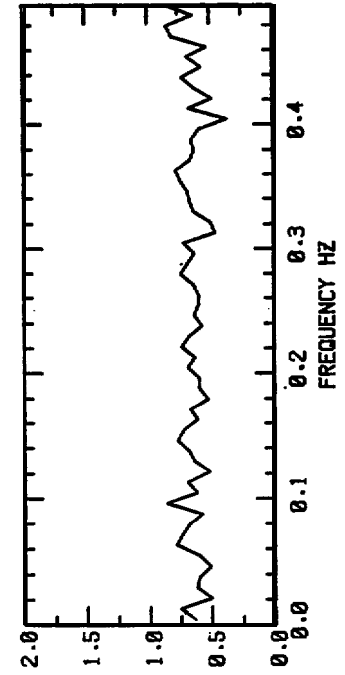


Figure 9c, d. Frequency response functions and coherence functions for floe-mounted accelerometer with reference to SEASPRI buoy,

of surface waves for the bounding depths of water as a function of period using

$$\lambda = \frac{g}{2\pi f^2 I\left(\frac{4\pi^2 f^2 h}{g}\right)}, \quad (12)$$

where $I\left(\frac{4\pi^2 f^2 h}{g}\right)$ is the iterative hyperbolic cotangent function introduced by Pierson (1955). Given that we know the separation between SEASPRI and the floe-mounted accelerometer (10 m), we may then compare the wavelength predicted by the theory with that computed from the phase factor of the measured time series. Figure 10 shows the results of this calculation; the data show reasonable agreement with the theoretical curves.

The Strain Data

In an earlier section we mentioned briefly that a single buoy could provide directional information only if it was able to measure tilt as well as sea surface elevation. One is tempted to ask whether a **wavebuoy** which could measure its own **flexural** surface strain field as well as sea surface elevation might also give some idea of the directional wave spectrum. In engineering applications this question is equivalent to asking whether it is possible to locate the axes of principal strain and compute the two principal strains for a body with some arbitrary strain field. This involves the use of a strain rosette whereby three instruments are placed at a known angle to one another so that the three unknowns may be computed from the individual strain records. A variety of rosette configurations exist and these are discussed fully in the engineering literature (see for example, Meier, 1950; Holister, 1967). We use the so-called delta (120°) rosette since at the outset of the experiment, one has no knowledge about the

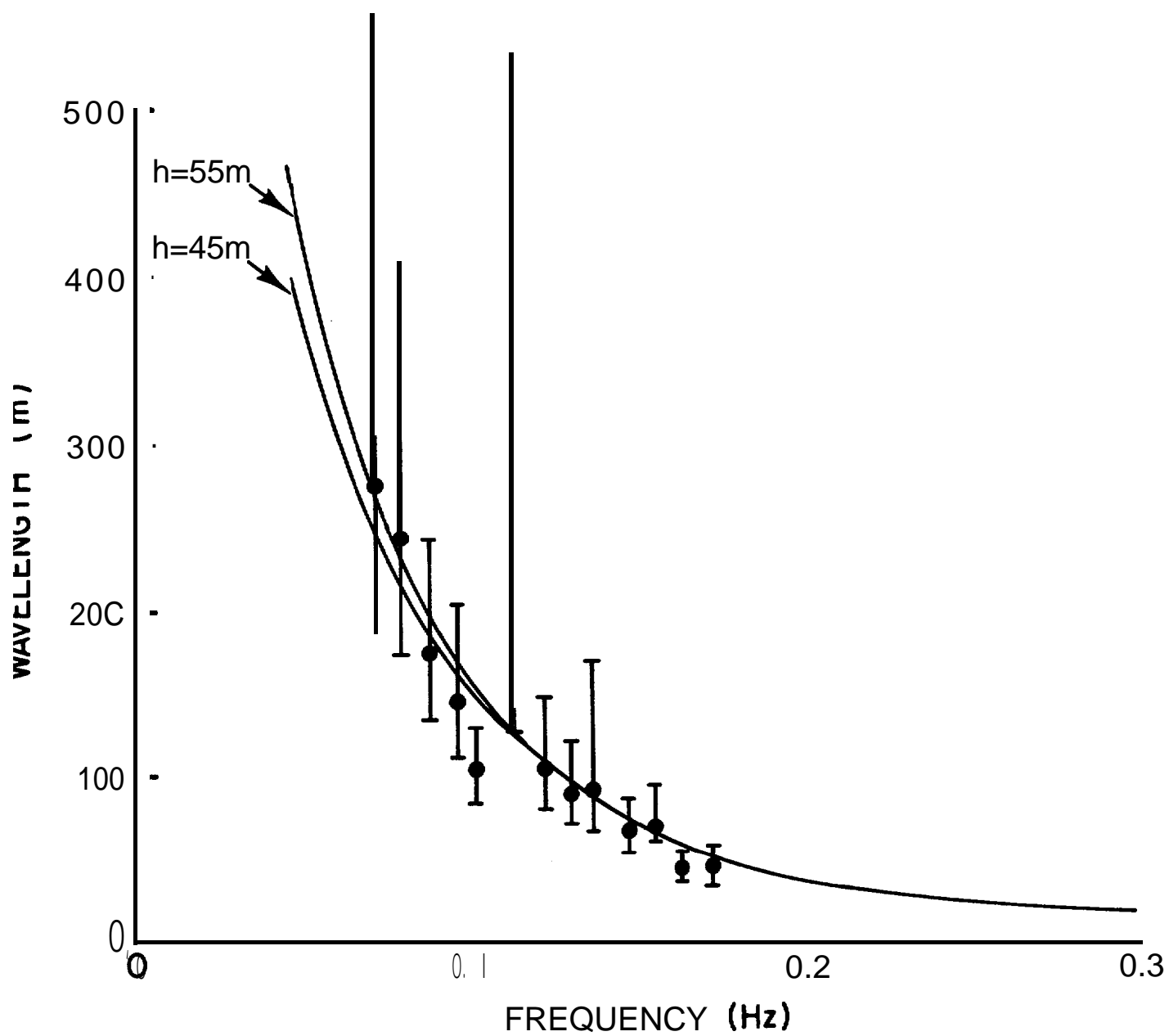


Figure 10. Comparison of experimental and theoretical curves for wavelength versus wave frequency.

direction of propagation of the significant waves. The precise configuration chosen, however, is unimportant. In this section we will discuss two possible directional interpretations of the strain data which may be developed into an order-of-magnitude estimate of the surface strain required to fracture our floe, and probably Bering Sea floes in general. We begin however with a brief general discussion on the appearance of the strain spectra.

Typical strain power spectra are shown in Figures 11a and b alongside the corresponding time series. The spectra were derived in a similar way to previous spectra but with no correction to energy density. The vertical units are therefore microstrain^2 s where **microstrain** is given by (extension/original length) $\times 10^{-6}$. The strain time series are precisely synchronized with the equivalent SEASPRI and floe-mounted accelerometer records. Examination of the figures shows that the spectra are much broader than previous power spectra, with their spectral peakedness $Q_p < 1.5$ compared with $Q_p > 3$ for the heave spectra. In fact it is tempting to ask where the additional high frequency energy shown in the strain spectra comes from. The argument is similar to that for the acceleration correction: Consider the floe to bend perfectly to the waves so that the curvature of its neutral axis and the sea surface are equal. Then, if we suppose that the ice floe is of thickness H and is isotropic, and for simplicity we treat a single wave mode as before, viz.,

$$y_n = A_n \cos 2\pi \left(\frac{x}{\lambda_n} - f_n t + \alpha_n \right) \quad , \quad (13)$$

we may calculate the modal surface strain E_n on the ice floe as

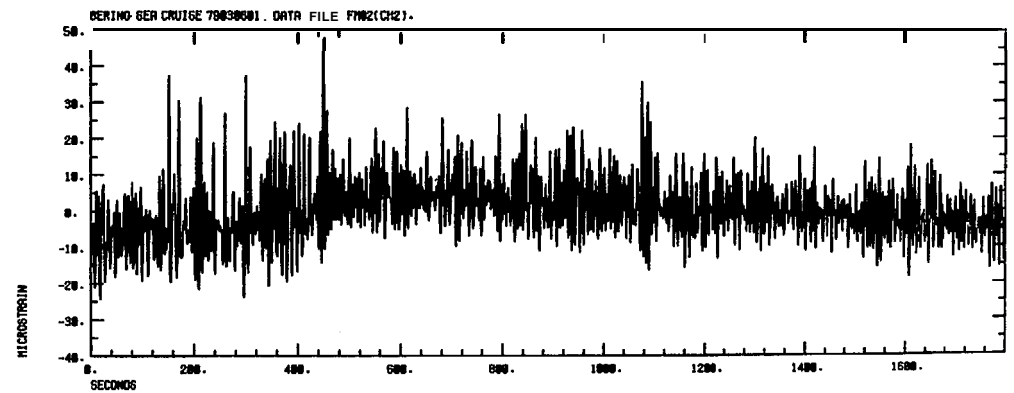
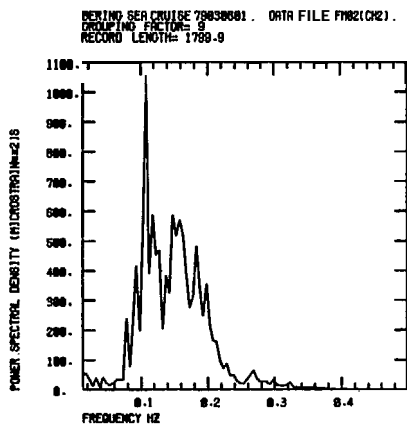
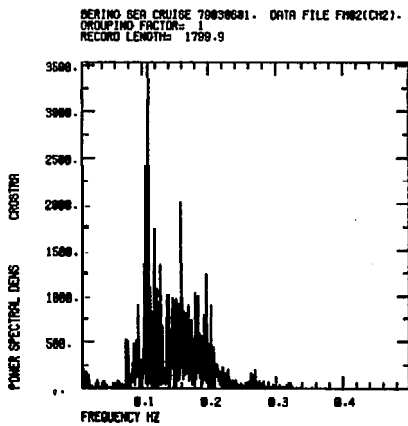
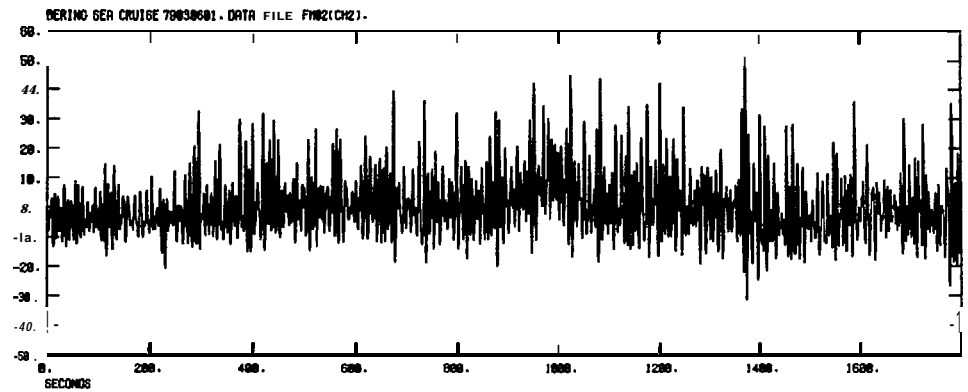
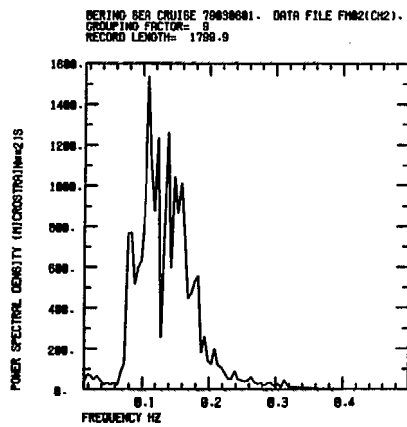
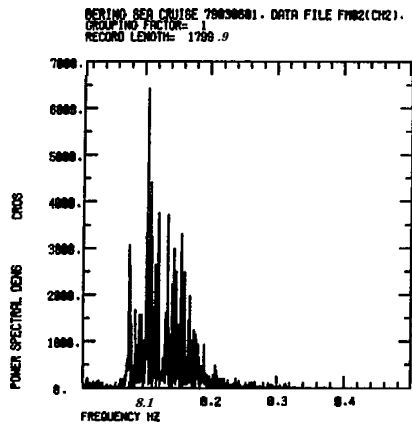


Figure ha, b. Strain spectra and time series for strainmeter 2.
The time series are synchronized with Figure 7e, f.

$$\epsilon_n = \frac{-H}{2} \frac{\partial^2 y_n}{\partial x^2} = \frac{H}{2} \left(\frac{2\pi}{\lambda_n} \right)^2 y_n \quad . \quad (14)$$

Alternatively, the wavelength may be related to frequency using equation (12) so that

$$\epsilon_n = \frac{8\pi^4 f_n^4 H}{g^2} I^2 \left(\frac{4\pi^2 f_n^2 h}{g} \right) y_n \quad . \quad (15)$$

Since we have already computed the theoretical relationship between **wave-**length and frequency in finite depth of water h (Figure 10), the breadths of the strain spectra are best interpreted using equation (14). As frequency increases, λ_n decreases so that A_n^{-2} increases rapidly. Hence, a strain spectrum will tend to be broad because its high frequency components are significantly enhanced.

From equation (15) it is in principle possible to derive the corresponding PSD for sea surface displacement. However, this calculation would **pre-**assume isotropy, so that since we are interested in relating our data to a fracture strain, the spectra have been left as strain spectra. The area beneath a strain spectrum therefore represents mean-square surface strain.

The simplest approach to obtaining some idea about the directionality of the strain field is to relate a spectrum from each strainmeter to the equivalent **SEASPRI** spectrum by means of the frequency response function defined **earlier**. This computation has been carried out and the results are shown in Figures 12a, b, and c where the gain factors for each instrument relative to **SEASPRI** are plotted. In this case a gain factor of unity does not imply a perfect bending response because of the reasons outlined above. To normalize the bending response, it is first necessary to correct by multiplication of the gain factor $|H(\mathbf{f})|$ by

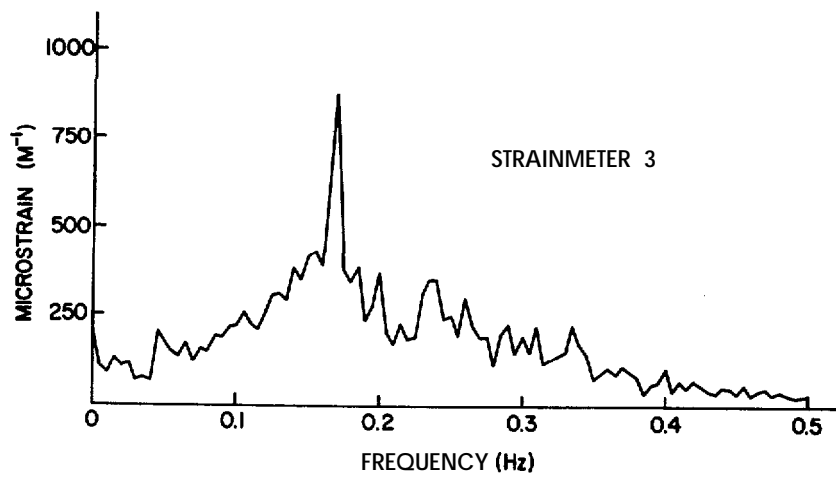
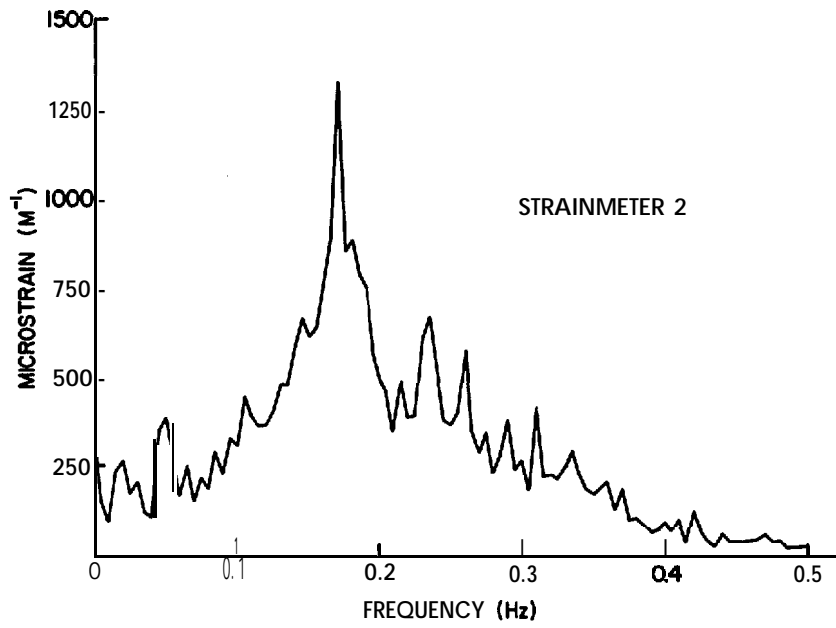
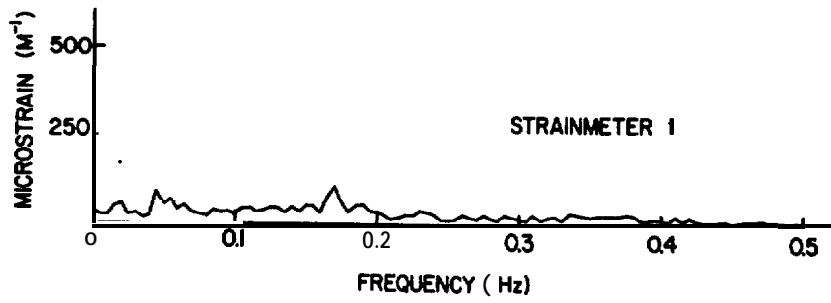


Figure 12a, b, c. Gain factors for strainmeters 1, 2, and 3 with respect to SEASPRI buoy.

If this is carried out, the bending response in each of the three **strain-** meters may be found and hence the angular division of energy so long as floe rotation is negligible. Observations during the experiment show this to be the case. It is found that most of the energy in the open water is propagating from between 200° and 220° and that the directional spread is extremely small.

An alternative, and better approach to finding the direction of the strain field is to take advantage of the wealth of literature in the engineering textbooks on strain gauge rosettes. Then for a delta rosette the principal strains ϵ_A, ϵ_B , and the direction of the axes of principal strain θ are given by

$$\epsilon_A + \epsilon_B = \frac{2}{3}(\epsilon_1 + \epsilon_2 + \epsilon_3) \quad ,$$

$$\epsilon_A - \epsilon_B = \frac{4}{3} (\epsilon_1^2 + \epsilon_2^2 + \epsilon_3^2 - \epsilon_1\epsilon_2 - \epsilon_2\epsilon_3 - \epsilon_3\epsilon_1)^{1/2} \quad ,$$

$$\tan 2\theta = \frac{\sqrt{3}(\epsilon_1 - \epsilon_2)}{2\epsilon_1 - \epsilon_2 - \epsilon_3} \quad \dots \quad 16)$$

where ϵ_1, ϵ_2 , and ϵ_3 are the strains measured by strainmeters 1, 2, and 3, and θ is measured from strainmeter 1 (Jaeger, 1956). Due to **the** slight phase lag introduced by instrument separation, the principal strains must be computed from the power spectra rather than directly from the strain time series. This may easily be seen if one considers a single monochromatic wave mode traveling along the axis of one of the gauges, then the other two instruments will experience the same displacement slightly after the first

strainmeter. An extreme case is when the strain measured by the first strainmeter averages out to zero, then the standard rosette calculation will produce erroneous results for the principal strains. In this case the angle θ is computed correctly, but when waves of arbitrary alignment are permitted, or worse a random short-crested sea, significant errors will be introduced in all the computed principal strain parameters. The alternative analysis is outlined in Squire (1978) where it is applied to flexural-gravity waves in fast ice.

The strain data for the floe have been analyzed using Squire's method to compute a spectrum of angular variation and amplitude spectra for each principal strain. To derive the spectra, small frequency bandwidths were chosen (nine contiguous spectral values) and the root-mean-square strains were calculated at the center frequency of each bandwidth. These values were then used in equations (16) to derive ϵ_A , ϵ_B and e as functions of frequency. Implicit in the analysis is that floe rotation may be neglected. This is believed to be a reasonable assumption in the present case since none of the strain records significantly changed in amplitude with time.

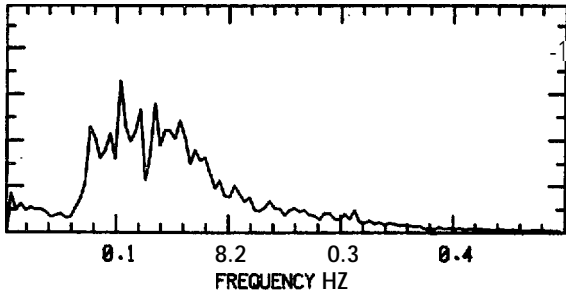
Figures 13a, b, c, and d show the principal strain amplitude spectra and the angle spectrum for the four strain experiments. It is important to realize that these are amplitude spectra (equivalent to Fourier transforms) and not power spectra though each spectral value does have some statistical meaning. The significant strain cannot be computed from this type of spectrum easily however.

The principal strain ϵ_A is over an order of magnitude greater than ϵ_B . This indicates that the strain field has little directional spread since most of the energy is exciting strain in a very narrow angular band.

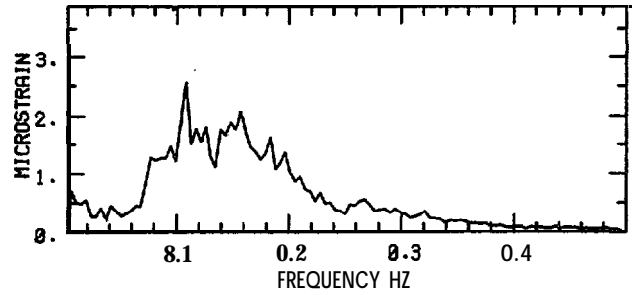
BERING SEA CRUISE 73S3SS1 . DATA FILE FM02(CH1).
 BERING SEA CRUISE 79030601 . DATA FILE FM02(CH2).
 BERING SEA CRUISE 79030601 . DATA FILE FM02(CH3).
 GROUPING FACTOR 9

BERING SEA CRUISE 79038S91 . DATA FILE FM02(CH1).
 BERING SEA CRUISE 7983SS01 . DATA FILE FM02(CH2).
 BERING SEA CRUISE 79030601 . DATA FILE FM02(CH3).
 GROUPING FACTOR 9

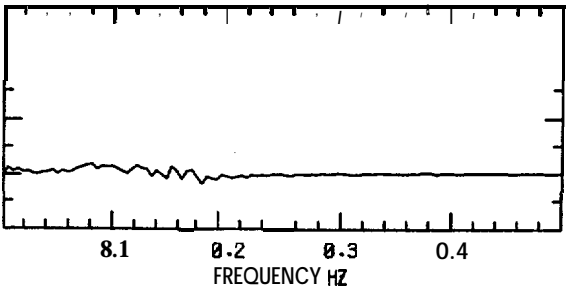
EPSILON1



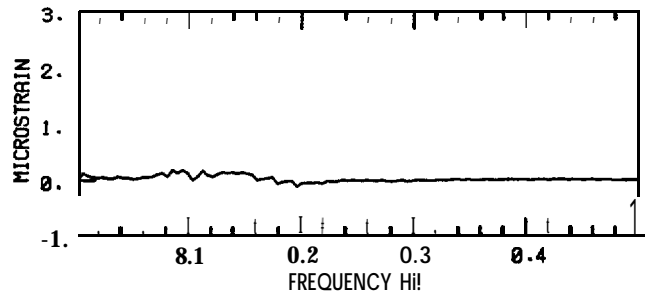
EPSILON1



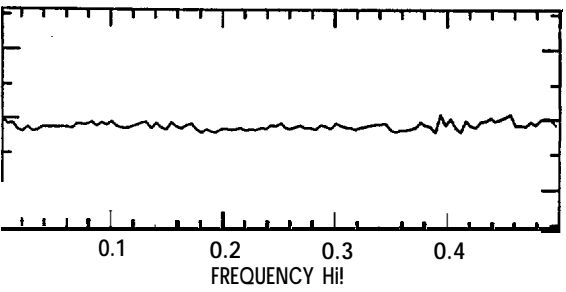
EPSILON2



EPSILON2



GAMMA



GAMMA

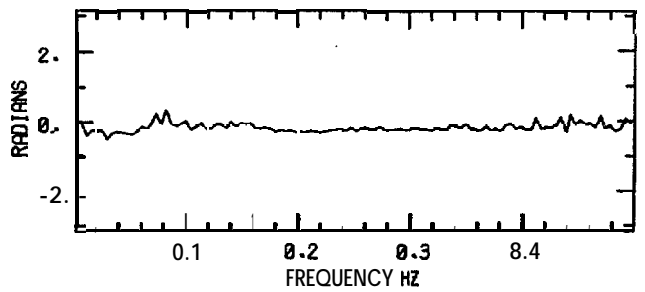
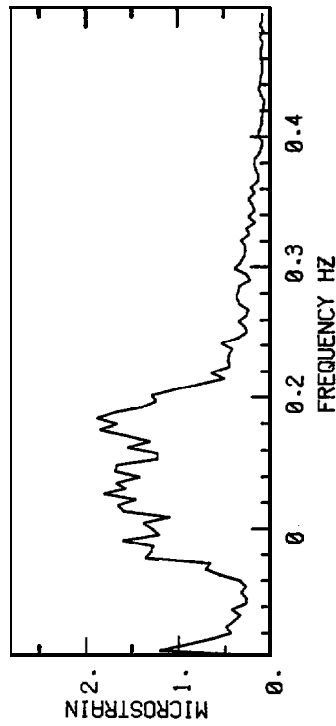


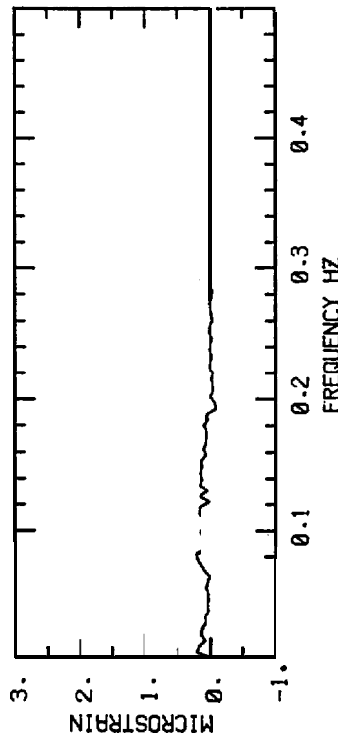
Figure 13a, b. Amplitude spectra for principal strains and principal strain direction. Experiments began at a) 10.38 and b) 11.08.

BERING SEA CRUISE 79030602. DATA FILE FM02(CH1).
 BERING SEA CRUISE 79030602. DATA FILE FM02(CH2).
 BERING SEA CRUISE 79030602. DATA FILE FM02(CH3).
 GROUPING FACTOR 9

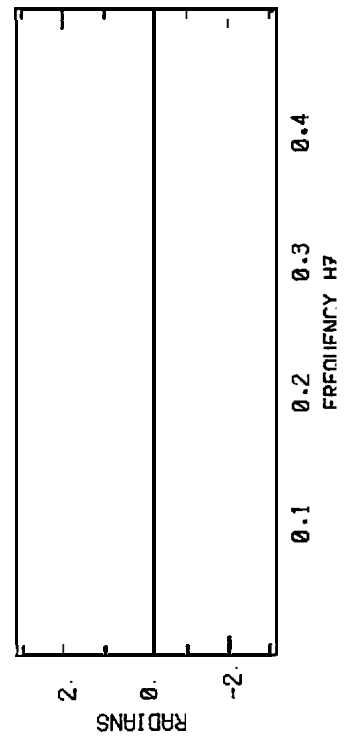
EPSILON1



EPSILON2

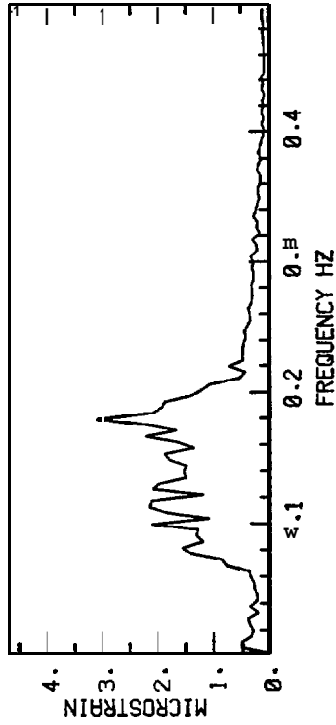


GAMMA

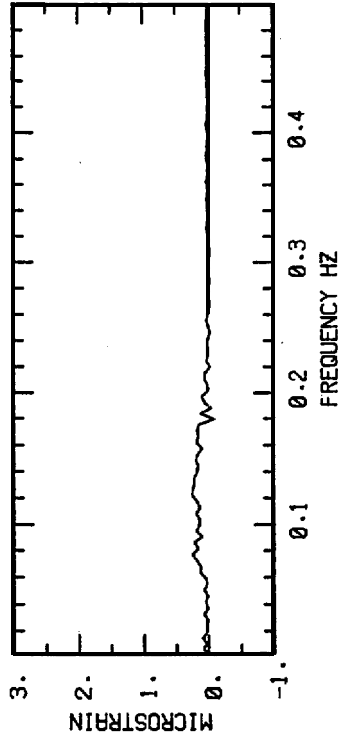


BERING SEA CRUISE 79030602. DATA FILE FM02(CH1).
 BERING SEA CRUISE 79030602. DATA FILE FM02(CH2).
 BERING SEA CRUISE 79030602. DATA FILE FM02(CH3).
 GROUPING FACTOR 9

EPSILON1



EPSILON2



GAMMA

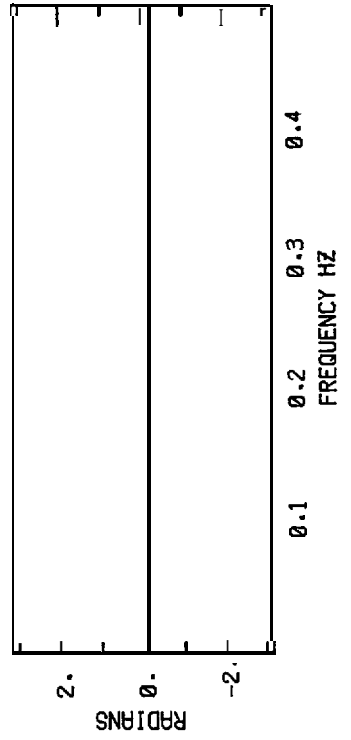


Figure 13c, d. Amplitude spectra for principal strains and principal strain direction. Experiments began at c) 11.56 and d) 12.26.

The angle of propagation of the strain wave may therefore be formed from the amplitude spectrum for θ . Once again we are lucky. The angle θ is remarkably constant over frequency (though it certainly doesn't have to be) and for the first experiment has a standard deviation **of only 4.4° about a mean which gives waves propagating from 200°**. This agrees well with our observations, the ship's log, and the direction predicted roughly by the earlier analysis. Later experiments give the same direction of propagation though the onset of short period wave activity makes the spectra noisier and increases the variance of wave direction with frequency.

The strain rosette analysis has therefore led to two conclusions: first that the measured ocean wave spectra have a very **small** angular spread, and second that the waves are propagating from a direction of about 200° irrespective of frequency. **This is not too surprising** since during the experiment the wind, waves, and swell directions coincided.

Our final interpretation of the strain data relies heavily on the work of Cartwright and Longuet-Higgins (1956) who developed a statistical model which could be used to find an estimate of a random function subsequent to the measured record. The methodology is outlined very simply in Draper (1963) and Tann (1976). Initially certain assumptions about the random function have to be made:

- (i) The function is considered as the 'superposition of infinitely **many sinusoids of random phase**.
- (ii) The spectrum is narrow. This is necessary to relate the distribution of zero up-cross waves and the **zeroth** spectral moment **(Tann, 1976)**.
- (iii) The random function is stationary.

It is clear that conditions (ii) and (iii) are questionable. However, we shall proceed on the understanding that any subsequent analysis can produce only an order-of-magnitude estimate.

The fundamental motivation behind our work is that we know that our **floe did not fracture while we were measuring strain but did fracture within an hour or so of our leaving. We may therefore compute the significant strain** for the recorded time series and call this our lower bound. The upper bound may then be found using **Tann's** analysis to calculate a "projected estimate" of strain over a time which includes the floe fracture. Both calculations are adjusted so that the strain is estimated in the wave direction found by the rosette analysis with the understanding that the angle of propagation does not change much with frequency.

The significant strains from each **rosette** give maximum principal strain values of 44, 36, 34, 40 μ **strain** so we shall take our lower bound as 44 μ **strain**. Following **Tann's** analysis to compute the maximum principal strain likely to occur in three hours around the recorded data, we find

$$\epsilon_{\max}(3 \text{ hour}) = \sqrt{8 m_0 \psi} \quad , \quad (17)$$

where ψ is the solution of

$$\psi = \ln N - \ln \left[1 - \frac{1}{2\psi} (1 - e^{-\psi}) \right] \quad . \quad (18)$$

In this equation N represents the expected number of zero up-cross waves in three hours, that is

$$N = \frac{3 \times 60 \times 60}{T_z} \quad . \quad (19)$$

From equation (17) we compute the maximum projected principal strain values for the four experiments as 85, 69, 66, and 78 μstrain so that our choice for the upper bound on surface strain is taken as 85 μstrain . Hence, tentatively, we write

$$44 < \epsilon < 85 \mu\text{strain} . \quad (20)$$

Unfortunately, the authors know of no *in situ* measurements of fracture strain for Bering Sea ice. The only *in situ* measurement where the surface strain at fracture was measured directly took place in east Greenland in 1978 when a **multiyear** floe broke up due to the action of waves during an experiment similar to those carried out in the Bering Sea (Goodman *et al.*, 1980). A value of 43 μstrain was measured in this case though the instrument used to record the **strain** is likely to have over-estimated its value (Moore and Wadhams, 1980). Our bounds for Bering Sea ice then seem reasonable given that the ice is thinner and warmer than the east Greenland floes and so is able to bend more easily to the sea surface profile. As Goodman *et al.* (1980) point out however, it is not possible to define either a universal fracture strain ϵ or a universal strength for sea ice. This is because the distribution and length of cracks within the material and its structure control ϵ . Since sea ice is a composite material made up of brine inclusions and drainage channels within a matrix of ice crystals, the sea ice structure is closely linked to its growth history. Hence the value of ϵ measured on the floe is strictly not applicable to sea ice in general. We suspect however, that our measured fracture strain is valid for floes of a similar growth history, as exist near the Bering Sea ice edge.

DISCUSSION

A simple model for the **flexural** response of ice floes which neglects the added mass, damping, and diffraction effects of a floating body has been successfully applied to ice islands by Goodman *et al.* (1980). The model calculates the **flexural** surface strain by first imposing the condition that the water motions do not see the floating rigid body, then allowing the body to bend elastically on the pressure field. Despite its **simpli-**city, the model gave good agreement with the ice island data. Using the two fracture bounds calculated for our floe the Goodman *et al.* model has been used to compute Figure 14. The graph is a plot of the wave steepness ak , where a is amplitude and k is wave number necessary to obtain surface **strain** values of 44 and 85 **μ strain** for the floe as a function of incident wave period. The figure may be divided into four zones: zone I where the strains never exceed 44 **μ strain** so that fracture "can never occur"; zone II where the surface strain lies within the two bounds so that fracture is possible; zone III where the floe would immediately fracture; and zone IV where the wave steepness ak exceeds 0.45, which is not possible for water waves (Kinsman, 1965). The presence of zone IV has **important consequences, namely that waves of periods outside a range --3 s to .19 s can never break our floe since waves of such steepness cannot exist oceanographically.** It must be remembered however that Figure 14 is strictly only valid for our floe, since changes in floe diameter and floe thickness have considerable effect on the surface strain. As floe diameter increases, the surface strain will increase to an asymptotic value which depends on floe thickness; as floe thickness increases, surface strain decreases. Large **floes** of a given thickness can therefore only exist so long as the forcing-wave amplitudes do not produce surface

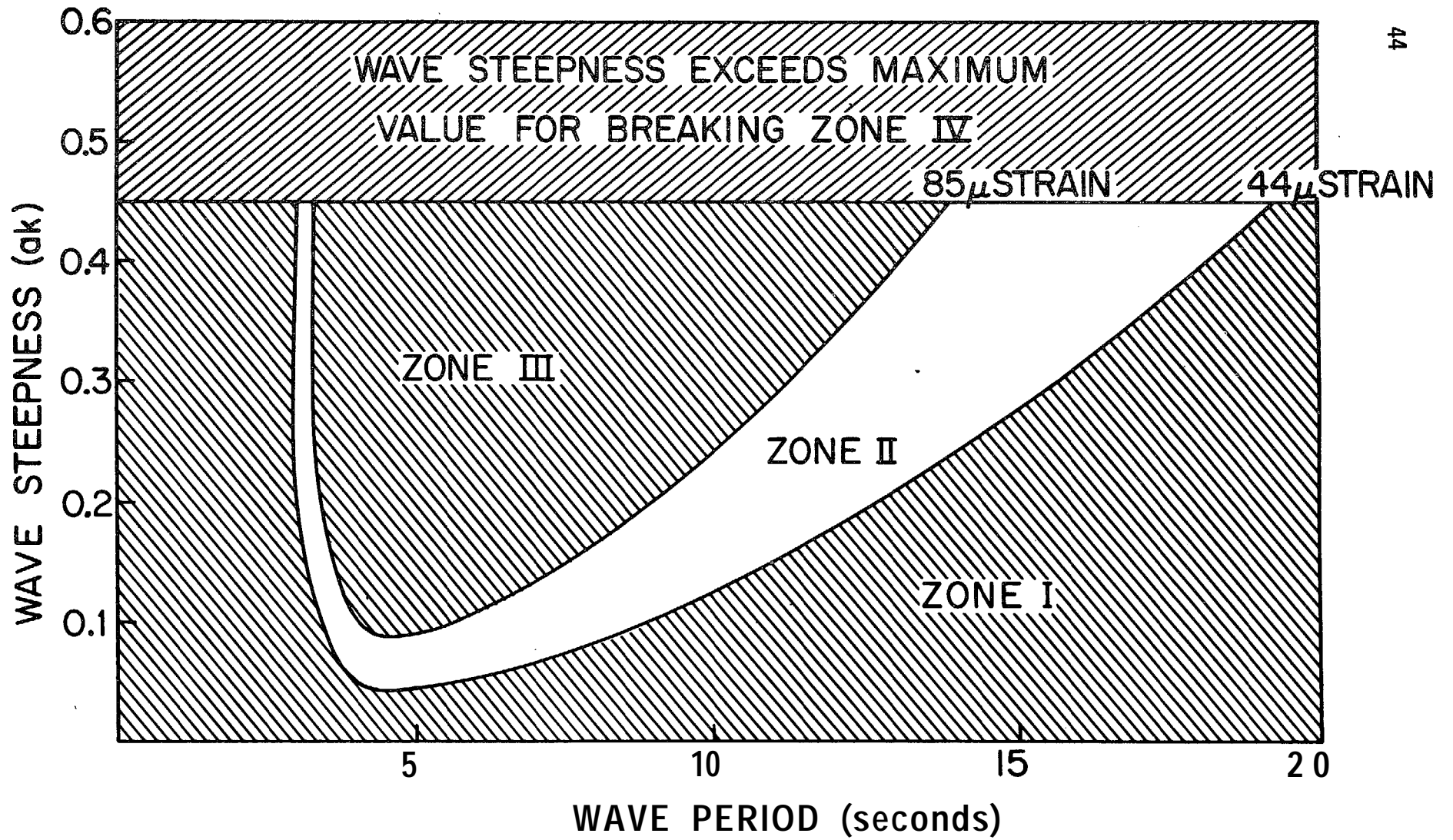


Figure 14. Wave steepness necessary to produce strains of 44 and 85 μstrain at surface of the floe as a function of wave period.

ACKNOWLEDGEMENTS

The authors gratefully acknowledge the assistance of Peter Kauffman and Stuart Moore in the field work and of Ray Home for the development of the computer package used in the data analysis. We thank Dr. David Halpern of the Pacific Marine Environmental Laboratory for the loan of the Waverider buoy, Jane Bauer for the preliminary analysis of the Waverider tapes, and the officers and crew of the NOAA ship SURVEYOR for their very great help. We also acknowledge the support of the Office of Naval Research under Contracts N00014-78-G-0003 and **N00014-76-C-0234**, and **V.A.S.** acknowledges the support of the British Petroleum Company Ltd. Much of this study was supported by the Bureau of Land Management through an interagency agreement with the National Oceanic and Atmospheric Administration, under which a **multiyear** program responding to the needs of petroleum development of the Alaskan continental shelf is managed by the Outer Continental Shelf Environmental Assessment Program (**OCSEAP**) Office.

REFERENCES

- Bauer**, J. and S. Martin, 1980. Field observations of the Bering Sea ice properties during March 1979. *Monthly Weather Review* (submitted).
- Bendat, J. S. and A. G. **Piersol**, 1971. *Random Data: Analysis and Measurement Procedures*, Wiley - **Interscience**, New York, 407 pp.
- Bingham**, C., M. D. Godfrey, and J. W. Tukey, 1967. Modern techniques of power spectrum estimation. *Trans. IEEE Audio and Electroacoustics*, *AU-15* (2), 56-66.
- Cartwright, D. E. and M. S. Longuet-Higgins, 1956. The statistical distribution of the maxima of a random function. *Proc. R. Soc. Lond. A.*, *237*, 212-232.
- Cooley**, J. W. and J. W. Tukey, 1965. An algorithm for the machine calculation of complex Fourier series. *Math Comput.*, *19*, 297-301.
- Draper, L., 1963. Derivation of a 'design wave' from instrumental records of sea waves. *proceedings of the Institute of Civil Engineers*, Vol. 26, 291-304.
- Frankenstein, G. and R. Garner, 1967. Equations for determining the brine volume of sea ice from -0.5° to -22.9°C . *J. Glaciol.*, *6* (48), 943-944.
- Goda, Y., 1970. Numerical experiments on wave statistics with spectral simulation. *Report of the Port and Harbour Institute*, Vol. 9, No. 3, 57 pp.
- Goodman, D. J., P. **Wadhams**, and V. A. Squire, 1980. The **flexural** response of a tabular ice **island** to ocean swell. Paper presented at Second Conference on the Use of Icebergs, 1-4 April, Cambridge University, England.
- Holister**, G. S., 1967. *Experimental Stress Analysis, Principles and Methods*, Cambridge Engineering Series, ed. Sir John Baker, Cambridge University Press, Cambridge, England, 62-76.

- Jaeger, J. C., 1956. *Elasticity, Fracture and Flow with Engineering and Geological Applications*, Methuen and Co., Ltd., New York, 152 pp.
- King, J. C. P. and R. G. Bilham, 1973. Strain measurements instrumentation and techniques. *Phil. Trans. R. Soc. A.*, 274, 209-217.
- Kinsman, B., 1965. *Wind Waves*, Prentice-Hall, Inc., Englewood Cliffs, New Jersey, 676 pp.
- Lathi, B. P., 1965. *Communication Systems*, John Wiley and Sons, Inc., New York, 431 pp.
- Lee, C. M., 1976. Motion characteristics of floating bodies. *J. Ship Res.*, 20 (4), 181-189.
- McNutt, S. L., 1980. Remote sensing analysis of the ice regime in the eastern Bering Sea. *Monthly Weather Review* (submitted).
- Meier, J. H., 1950. Strain rosettes. In: *Handbook of Experimental Stress Analysis*, ed. M. Hetényi, John Wiley & Sons, New York, 390-437.
- Moore, S. C. and P. Wadhams, 1980. Recent developments in strainmeter design. Workshop on stress and strain measurement in ice, Memorial University, St. John's, Newfoundland, Canada, 29 April - 2 May 1980. (Proceedings in press.)
- Pierson, N. J., Jr., 1955. Wind generated gravity waves. *Adv. Geophys.*, 2, Academic Press, Inc., New York, 93-178.
- Pitt, E. G., J. S. Driver, and J. A. Ewing, 1978. *Some Comparisons Between Wave Records*, Institute Oceanographic Sciences Report No. 43, 63 pp.
- Schwarz, J. and W. F. Weeks, 1977. Engineering properties of sea ice. *J. Glaciol.*, 19 (81), 499-531.
- Squire, V. A., 1978. An investigation into the use of strain rosettes for the measurement of propagating cyclic strains. *J. Glaciol.*, 29 (83), 425-431.
-

- ✓ Squire, V. A. and S. C. Moore, 1980. Direct measurement of the attenuation of ocean waves by pack ice. *Nature, London*, 283 (5745), 365-368.
- Tann, H. M., 1976. *The Estimation of Wave Parameters for the Design of Offshore Structures, a description of the method presently used by IOS*, Institute of Oceanographic Sciences Report No. 23, 29 pp.
- Wadhams, P., 1973. *The Effect of a Sea Ice Cover on Ocean Surface Waves*, Ph.D. dissertation, University of Cambridge, England, 223 pp.
- Wadhams, P., 1980. The ice cover in the Greenland and Norwegian Seas. Unpublished report, Scott Polar Research Institute.
- Wadhams, P. and V. A. Squire, 1980. Field experiments on wave-ice interaction in the Bering Sea and Greenland waters, 1979. *Polar Record* (in press).

DISTRIBUTION LIST

51

CONTRACT N00014-76-C-0234
NR 307-252

DEFENSE DOCUMENTATION CENTER
CAMERON STATION
ALEXANDRIA, VA 22314

US NAVAL RESEARCH LABORATORY
CODE 2627
WASHINGTON, DC 20375

WOODS HOLE OCEANOGRAPHIC INST
DOCUMENT LIBRARY LO-206
WOODS HOLE, MA 02543

COLD REGIONS RES & ENG LAB
PO BOX 282
HANOVER, NH 03755

CAPT D C NUTT, USN (RET)
DEPARTMENT OF GEOGRAPHY
DARTMOUTH COLLEGE
HANOVER, NH 03755

DR JOHN C F TEDROW
DEPT OF SOILS, LIPMAN HALL
RUTGERS UNIVERSITY
NEW BRUNSWICK, NJ 08903

DR KENNETH L HUNKINS
LAMONT-DOHERTY GEOLOGICAL OBSY
TORRY **CLIFFE**
PALISADES, NY 10964

CHIEF OF ENGINEERS
ATTN **DAEN-MCE-D**
DEPARTMENT OF THE ARMY
WASHINGTON, DC 20314

DEPARTMENT OF THE ARMY
OFFICE CHIEF OF ENGINEERS
ATTN DAEN-RDM
WASHINGTON, DC 20314

MR M R HERRMAN
NAVAL FACILITIES ENG COMMAND
CODE 032 A, YARDS & DOCKS ANNEX
ROOM 2B1
WASHINGTON, DC 20390

MR ROBERT D KETCHUM JR
BLDG 70, CODE 8050
NAVAL RESEARCH LABORATORY
WASHINGTON, DC 20390

MR LOUIS DEGOES, EXEC **SECTY**
POLAR RESEARCH BOARD
NATL ACADEMY OF SCIENCES
2101 CONSTITUTION AVENUE, NW
WASHINGTON, DC 20418

POLAR INFORMATION SERVICE
OFFICE OF POLAR PROGRAMS
NATIONAL SCIENCE FOUNDATION
WASHINGTON, DC 20550

DR GEORGE A LLANO
ACTING CHIEF SCIENTIST
OFFICE OF POLAR PROGRAMS
NATIONAL SCIENCE FOUNDATION
WASHINGTON, DC 20550

MRMM **KLEINERMAN**
PROJECT MANAGER FOR ARCTIC ASW
US NAVAL ORDNANCE LABORATORY
WHITE OAK, MD 20910

MR PAUL P LAUVER, PUBLICATIONS
ARCTIC **INST** OF NORTH AMERICA
3426 NO WASHINGTON BLVD
ARLINGTON, VA 22201

DR G LEONARD JOHNSON
CODE 461, ARCTIC PROGRAMS
OFFICE OF NAVAL RESEARCH
ARLINGTON, VA 22217

DR NORBERT UNTERSTEINER
SCI ADV FOR ARCTIC & POLAR AFFAIRS
OFFICE OF NAVAL RESEARCH
CODE 400P
ARLINGTON, VA 22217

CHIEF OF NAVAL RESEARCH
OFFICE OF NAVAL RESEARCH
CODE 412
ARLINGTON, VA 22217

CHIEF OF NAVAL RESEARCH
OFFICE OF NAVAL RESEARCH
CODE 414
ARLINGTON, VA 22217

CHIEF OF NAVAL RESEARCH
OFFICE OF NAVAL RESEARCH
CODE 480D
ARLINGTON, VA 22217

52 DISTRIBUTION LIST, CONTRACT N00014-76-C-0234, NR 307-252

US NAVAL OCEANOGRAPHIC OFFICE
LIBRARY (CODE 8160)
NSTL STATION
BAY ST LOUIS, MS 39522

DIRECTOR, INST OF POLAR STUDIES
OHIO STATE UNIVERSITY
125 SOUTH OVAL DRIVE
COLUMBUS, OH 43210

DR ALBERT H JACKMAN
CHAIRMAN, DEPT OF GEOGRAPHY
WESTERN MICHIGAN UNIVERSITY
KALAMAZOO, MI 49001

DR REID A BRYSON
INST FOR ENVIRONMENTAL STUDIES
UNIVERSITY OF WISCONSIN
MADISON, WI 53706

DR DAVID CLARK
DEPARTMENT OF GEOLOGY
UNIVERSITY OF WISCONSIN
MADISON, WI 53706

PROF RICHARD S TANKIN
DEPT OF MECH ENGINEERING
NORTHWESTERN UNIVERSITY
EVANSTON, IL 60201

PROF WILLIAM MCINTIRE
COASTAL STUDIES INSTITUTE
LOUISIANA STATE UNIVERSITY
BATON ROUGE, LA 70803

DR HARLEY J WALKER
DEPARTMENT OF GEOGRAPHY
LOUISIANA STATE UNIVERSITY
BATON ROUGE, LA 70803

DR V P HESSLER
4230 EUTAW STREET
BOULDER, CO 80302

WORLD DATA CENTER: A FOR GLAC
INST OF ARCTIC & ALPINE RESEARCH
UNIVERSITY OF COLORADO
BOULDER, CO 80309

CONTRACT ADMINISTRATOR
OFFICE OF NAVAL RESEARCH BRANCH OFC
1030 EAST GREEN STREET
PASADENA, CA 91106

COMMANDER
NAVAL UNDERSEA CENTER
ATTN TECHNICAL LIBRARY, CODE 1311
SAN DIEGO, CA 92132

RESEARCH LIBRARY
NAVAL ELECTRONICS LAB CENTRE
SAN DIEGO, CA 92152

LIBRARIAN
TECHNICAL LIBRARY DIVISION
NAVAL CIVIL ENGINEERING LABORATORY
PORT HUENEME, CA 93041

COMMANDING OFFICER
CODE L61
NAVAL CIVIL ENGINEERING LABORATORY
PORT HUENEME, CA 93043

MR BEAUMONT BUCK
POLAR RESEARCH LABORATORY ING
123 SANTA BARBARA STREET
SANTA BARBARA, CA 93101

SUPERINTENDENT
NAVAL POSTGRADUATE SCHOOL
LIBRARY CODE 2124
MONTEREY, CA 93940

DR ARTHUR LACHENBRUCH
BRANCH OF GEOPHYSICS
US GEOLOGICAL SURVEY
345 MIDDLEFIELD ROAD
MENLO PARK, CA 94025

DRW M SACKINGER
DEPT OF ELECTRICAL ENGINEERING
UNIVERSITY OF ALASKA
FAIRBANKS, AK 99701

DR KEITH MATHER
705 GRUENING BUILDING
UNIVERSITY OF ALASKA
FAIRBANKS, AK 99701

DR CHARLES E BEHLKE, DIRECTOR
INST OF ARCTIC ENVIRONMENTAL ENG
UNIVERSITY OF ALASKA
COLLEGE, AK 99701

DR DONALD W HOOD
INST FOR MARINE SCIENCE
UNIVERSITY OF ALASKA
FAIRBANKS, AK 99701

DR GUNTER WELLER
GEOPHYSICAL INSTITUTE
UNIVERSITY OF ALASKA
COLLEGE, AK 99701

LIBRARIAN
NAVAL ARCTIC RESEARCH LABORATORY
BARROW, AK 99723

MGR INUVIK RESEARCH LABORATORY
BOX 1430
INUVIK, NORTHWEST TERRITORIES
XO E TO CANADA

DR SVENN ORVIG
MCGILL UNIVERSITY
DEPT OF METEOROLOGY
PO BOX 6070
MONTREAL 101, PQ, CANADA

MARINE SCIENCE CENTRE LIBRARY
MCGILL UNIVERSITY
PO BOX 6070
MONTREAL 101, PQ, CANADA

DR E R POUNDER
RUTHERFORD PHYSICS BUILDING
MCGILL UNIVERSITY
3600 UNIVERSITY STREET
MONTREAL, PQ H3A 2T8, CANADA

MRS GAIL HORWOOD
METEOROLOGY LIBRARY
MCGILL UNIVERSITY
MONTREAL 101, PQ, CANADA

DEPARTMENTAL LIBRARY-SERIALS
DEPT OF THE ENVIRONMENT
OTTAWA, ONTARIO K1A 0H3
CANADA

DEFENCE RESEARCH BOARD
DEPT OF NATIONAL DEFENCE
190 O'CONNOR STREET
OTTAWA, ONTARIO K1A 0Z3
CANADA

MISS MOIRA DUNBAR
DEFENCE RESEARCH ESTABLISHMENT
OTTAWA, NATL DEFENCE HEADQUARTERS
OTTAWA, ONTARIO K1A 0Z4, CANADA

DR ROBERT L RAUSCH
DEPT OF MICROBIOLOGY
W COLLEGE OF VET MEDICINE
UNIVERSITY OF SASKATCHEWAN
SASKATOON, SASK S7N 0W0, CANADA

DR E L LEWIS
FROZEN SEA RESEARCH GROUP
INSTITUTE OF OCEAN SCIENCES
9860 W SAANICH ROAD, PO BOX 6000
SIDNEY, BC V8L 4B2, CANADA

DR A R MILNE
DEFENCE RES ESTABLISHMENT PAC
FLEET MAIL OFFICE
VICTORIA, BC, CANADA

METEOROLOGICAL OFFICE LIBRARY
LONDON ROAD
BRACKNELL, BERKSHIRE, ENGLAND

DRT E ARMSTRONG
SCOTT POLAR RESEARCH INSTITUTE
CAMBRIDGE, CB 2 1ER, ENGLAND

THE LIBRARIAN
SCOTT POLAR RESEARCH INSTITUTE
CAMBRIDGE CB2 1ER, ENGLAND

DR MICHAEL KELLY
SCHOOL OF ENVIRONMENTAL SCIENCES
UNIVERSITY OF EAST ANGLIA
NORWICH NR4 7TJ, ENGLAND

NATIONAL INST OF OCEANOGRAPHY
WORMLEY, GODALMING
SURREY, ENGLAND

CENTRE NATL DE LA RECHERCHE SCI
LABORATOIRE DE GLACIOLOGIE
UNIVERSITY DE GRENOBLE 1
SERV DE GEOPHYS, 2, RUE TRES
CLOITRES 38-GRENOBLE, FRANCE

CENTRE D'ETUDES ARCTIQUES
ECOLE PARTIQUE DES HAUTES ETUDES
VI SECTION (SORBONNE)
6, RUE DE TOURNON, PARIS -6
FRANCE

DR KOU KUSUNOKI
POLAR RESEARCH CENTER
NATIONAL SCIENCE MUSEUM
KAGA 1-9-10, **ITABASHI-KU**
TOKYO, JAPAN

NORSK POLARINSTITUTT
ROLFSTANGVN 12, **POSTBOKS 158**
1330 OSLO LUFTHAVN
NORWAY

PROF DR ALEXSANDER KOSIBA
KATEFRA I OBSERWATORIUM
METEOROLOGIC I KLIMATOLOGII
UNIwersytetn WROCLAWSKIEGO
WROCLAW 9, U CMENTARNA 8
POLAND

STOCKHOLM UNIVERSITET
NATURGEOGRAFI SKA INSTITUTIONEN
BOX 680?
113 86 STOCKHOLM, SWEDEN

DR ING O MAGGIOLO
FACULTAD DE INGENIERIA
HERRERA Y REISSIG 585
MONTEVIDEO, URUGUAY

LIBRARY-CENTRE FOR NORTHERN
STUDIES AND RESEARCH
MCGILL UNIVERSITY
1020 PINE AVENUE WEST
MONTREAL, PQ H3A 1A2
CANADA

UNIVERSITY ARCHIVES
UNIVERSITY RECORDS SECTION BL-10
UNIVERSITY OF WASHINGTON
SEATTLE, WA 98195

RESIDENT REPRESENTATIVE
OFFICE OF NAVAL RESEARCH
ROOM 422, UNIV DISTRICT **BLDG JD-27**
UNIVERSITY OF WASHINGTON
SEATTLE, WA 98105

DR LAWRENCE COACHMAN
DEPARTMENT OF OCEANOGRAPHY WB-10
UNIVERSITY OF WASHINGTON
SEATTLE, WA 98195

DRT SAUNDERS ENGLISH
DEPARTMENT OF OCEANOGRAPHY WB-10
UNIVERSITY OF WASHINGTON
SEATTLE, WA 98195

DR KNUT AAGARD
DEPARTMENT OF OCEANOGRAPHY WB-10
UNIVERSITY OF WASHINGTON
SEATTLE, WA 98195

REPORT DOCUMENTATION PAGE		READ INSTRUCTIONS BEFORE COMPLETING FORM
REPORT NUMBER SCIENTIFIC REPORT NO. 18	2. GOVT ACCESSION NO.	3. RECIPIENT'S CATALOG NUMBER
TITLE (and Subtitle) A FIELD STUDY OF THE PHYSICAL PROPERTIES, RESPONSE TO SWELL, AND SUBSEQUENT FRACTURE OF A SINGLE ICE FLOE IN THE WINTER BERING SEA		5. TYPE OF REPORT & PERIOD COVERED SCIENTIFIC REPORT
		6. PERFORMING ORG. REPORT NUMBER
AUTHOR(s) VERNON A. SQUIRE AND SEELYE MARTIN		8. CONTRACTOR GRANT NUMBER(s) N00014-76-C-0234
PERFORMING ORGANIZATION NAME AND ADDRESS ARCTIC SEA AIR INTERACTION DEPARTMENT OF ATMOSPHERIC SCIENCES AK-40 UNIVERSITY OF WASHINGTON, SEATTLE, WA 98195		10. PROGRAM ELEMENT, PROJECT, TASK AREA & WORK UNIT NUMBERS NR 307-252
1. CONTROLLING OFFICE NAME AND ADDRESS OFFICE OF NAVAL RESEARCH CODE 461, ARCTIC PROGRAM ARLINGTON, VA 22217		12. REPORT DATE JULY 1980
		13. NUMBER OF PAGES 53
4. MONITORING AGENCY NAME & ADDRESS (if different from Controlling Office)		15. SECURITY CLASS. (of this report) UNCLASSIFIED
		15a. DECLASSIFICATION/DOWNGRADING SCHEDULE
5. DISTRIBUTION STATEMENT (of this Report) THE DISTRIBUTION OF THIS REPORT IS UNLIMITED		
7. DISTRIBUTION STATEMENT (of the abstract included in Block 20, if different from Report)		
8. SUPPLEMENTARY NOTES		
9. KEY WORDS (Continue on reverse side if necessary and identify by block number) MARGINAL ICE ZONE OCEAN SWELL AND PACK ICE BERING SEA FLEXURAL STRAIN		
10. ABSTRACT (Continue on reverse side if necessary and identify by block number) Surface strain and vertical heave response experiments were conducted for a single floe within the marginal ice zone of the winter Bering Sea. The strain was measured using an array of three strainmeters placed in a 120° rosette configuration, and the heave was computed from simultaneous records of vertical acceleration on the floe and in the water around the floe. Physical properties studies and underwater traverses by divers were also carried out for the floe. The data are presented and interpreted in the light of the subsequent floe fracture; the mean fracture strain amplitude ϵ is found to lie between 44 and		

,56

22. (cont.) 85 μ strain. A discussion of the directionality of the wave energy during the experiment is also given.